Copy No. 254

RM No. A8J04

NACA RM No. A8J04

NACA

RESEARCH MEMORANDUM

AERODYNAMIC STUDY OF A WING-FUSELAGE COMBINATION EMPLOYING A WING SWEPT BACK 63°.- CHARACTERISTICS AT A MACH NUMBER OF 1.53 INCLUDING EFFECT OF SMALL VARIATIONS OF SWEEP

By Robert T. Madden

Ames Aeronautical Laboratory
Moffett Field, Calif.

NATIONAL ADVISORY COMMITTEE FOR AERONAUTICS

WASHINGTON
January 26, 1949

NATIONAL ADVISORY COMMITTEE FOR AERONAUTICS

RESEARCH MEMORANDUM

AERODYNAMIC STUDY OF A WING–FUSELAGE COMBINATION EMPLOYING A WING SWEPT BACK 63°.– CHARACTERISTICS AT A MACH NUMBER OF 1.53 INCLUDING EFFECT OF SMALL VARIATIONS OF SWEEP

By Robert T. Madden

SUMMARY

Wind–tunnel tests have been performed at a Mach number of 1.53 to determine experimentally the longitudinal characteristics of a wing–fuselage combination which theory indicates should be capable of attaining maximum lift–drag ratios greater than 10 to 1 at moderate supersonic speeds. The wing had a leading–edge sweep of 63°, an aspect ratio of 3.42, a taper ratio of 0.25, and an NACA 64A006 section parallel to the plane of symmetry. The primary objectives of the investigation were to determine to what extent the theoretical maximum lift–drag ratio could be realized experimentally and to determine the static longitudinal stability characteristics. Secondary objectives included the evaluation of the effects of Reynolds number and small variations of sweep at a constant Mach number. To determine this latter effect, the wing panels were rotated about the midpoint of the root chord to obtain a variation of leading–edge sweep angle from 57.0° to 69.9°. In addition to the force tests, liquid–film studies were made to determine the nature of the boundary–layer flow.

At a Reynolds number of 0.62 million, the 63° wing configuration had a maximum lift–drag ratio of 6.7; whereas theory indicated a value of 10.1. Liquid–film studies revealed that the difference between experiment and theory was primarily due to separation of the laminar boundary layer which occurred even at zero lift. Although the linear theory indicated a fixed center–of–pressure position, the experimental results showed that the center of pressure varied with lift coefficient over approximately 20 percent of the mean aerodynamic chord. This difference was also attributed to the effects of separation. As might be expected, increased Reynolds number had a marked influence on the extent of separation and

consequently on the measured aerodynamic characteristics. Increasing the Reynolds number to 0.84 million increased the maximum lift–drag ratio to 7.2 and reduced the total center–of–pressure travel to approximately 12 percent of the mean aerodynamic chord.

In the determination of the effects of sweep, it was found that the sweep angle for maximum lift–drag ratio was 67° for this general type of configuration at a Mach number of 1.53. Values of maximum lift–drag ratio of 7.1 and 7.4 were obtained at Reynolds numbers of 0.62 and 0.95 million, respectively. The optimum sweep angle resulted from the decrease in minimum drag coefficient and the increase in drag due to lift as the sweep angle was increased. The total center–of–pressure travel with lift coefficient increased with increasing angles of sweep.

The results of these tests indicate that further improvements in maximum lift–drag ratio and longitudinal stability may be expected at full–scale Reynolds numbers. However, since the large adverse lifting–pressure gradients may cause leading–edge separation even at high Reynolds numbers, the theoretical value of maximum lift–drag ratio may never be obtained with this wing. Therefore, the use of camber and twist to reduce the adverse gradient is indicated as a means of improving the boundary–layer flow characteristics and maximum lift–drag ratio.

INTRODUCTION

The possibility of attaining supersonic flight speeds without a large increase in fuel consumption per mile of flight over that required for level subsonic flight depends largely upon obtaining high lift–drag ratios at the desired flight Mach number. The theoretical aspects of efficient supersonic flight have been considered by Jones in reference 1. As a result of this theoretical study, it has been indicated that lift–drag ratios greater than 10 to 1 may be obtained up to a Mach number of approximately 1.5 by using large angles of sweepback and relatively high aspect ratios. Thus the thrust required and the fuel consumption for level supersonic flight near a Mach number of 1.5 should be considerably less than that necessary for straight–wing configurations which develop lift–drag ratios of approximately 6 to 1.

The most effective gains resulting from the use of sweepback at supersonic flight speeds are realized when the wing leading edge is swept behind the Mach lines originating at the apex of the wing

leading edge. An increase in maximum lift–drag ratio then results from decreases in both minimum drag coefficient and the drag due to lift. The effect of sweeping the wing leading edge well within the Mach cone in reducing the minimum drag coefficient has been shown by Jones in reference 2. The reduction in drag due to lift results from the realization of a leading–edge suction force associated with the up–flow at the wing leading edge that is not obtained with wings swept ahead of the Mach cone. The flow on the sections farthest from the wing root, exclusive of those within the tip Mach cones, most closely approach ideal, two–dimensional, subsonic flow and thereby realize the greatest reduction in minimum drag coefficient and drag due to lift. Thus the use of the highest practicable aspect ratio is indicated.

A general wind–tunnel investigation is being undertaken at the Ames Aeronautical Laboratory with wing–fuselage combinations having wings with leading edges swept back 63° to determine experimentally the characteristics of a configuration similar to the types shown by Jones in reference 1 to be theoretically efficient at supersonic flight speeds. The facilities employed permit a study at several Reynolds numbers for both subsonic and supersonic Mach numbers. Results obtained to date at subsonic speeds with this configuration are presented in references 3 and 4. The present investigation is primarily concerned with the characteristics of the 63° uncambered, untwisted wing and fuselage combination at a Mach number of 1.53. The leading–edge sweep angle in the present tests was variable within the range of 57.0° to 69.9° and, as a secondary phase of the study, an experimental determination of the optimum leading–edge sweep angle for maximum lift–drag ratio at a Mach number of 1.53 was undertaken. This secondary phase of the investigation also served to indicate any possible adverse effects, particularly on longitudinal stability characteristics, of a subsonic, sonic, or supersonic trailing edge.

SYMBOLS

Basic Symbols

A	aspect ratio $\left(\frac{b^2}{S}\right)$
b	wing span measured perpendicular to plane of symmetry, inches
c	wing chord measured parallel to plane of symmetry, inches

$\bar{c}$ mean aerodynamic chord $\left(\frac{\int_0^{b/2} c^2 dY}{\int_0^{b/2} c\, dY}\right)$, inches

$\bar{c}_g$ mean geometric chord $\left(\frac{S}{b}\right)$, inches

c_r wing root chord, inches

c_t wing tip chord, inches

C_D total drag coefficient $\left(\frac{\text{drag}}{q_o S}\right)$

$C_{D_{min}}$ minimum total drag coefficient

ΔC_D rise in drag coefficient above minimum $(C_D - C_{D_{min}})$

C_L lift coefficient $\left(\frac{\text{lift}}{q_o S}\right)$

$C_{L_{opt}}$ lift coefficient for maximum lift-drag ratio

$\frac{dC_L}{d\alpha}$ lift-curve slope, per radian unless otherwise specified

ΔC_L change in lift coefficient from value for minimum drag $\left(C_L - C_{L_{D=min}}\right)$

$\frac{\Delta C_D}{(\Delta C_L)^2}$ drag-rise factor

$\left(\frac{L}{D}\right)_{max}$ maximum lift-drag ratio

$C_{m_{\frac{1}{2}}}$ pitching-moment coefficient about 50 percent mean aerodynamic chord $\left(\frac{\text{pitching moment about 50 percent mean aerodynamic chord}}{q_o S \bar{c}}\right)$

$C_{m_{\frac{1}{4}}}$ pitching-moment coefficient about 25 percent mean aerodynamic chord $\left(\frac{\text{pitching moment about 25 percent mean aerodynamic chord}}{q_o S \bar{c}}\right)$

$\frac{dC_m}{dC_L}$ moment-curve slope

h location of maximum airfoil thickness, measured from leading edge in streamwise direction, inches

h/c chordwise location of maximum thickness t/c

k_a angle ratio, $\frac{\alpha_{\Delta L}}{\Delta \alpha}$

m ratio of the cotangent of sweep angle of the leading edge to the cotangent of the sweep angle of the Mach line

M_n Mach number corresponding to velocity component perpendicular to wing leading edge

M_o free-stream Mach number

P pressure coefficient $\left(\frac{p-p_o}{q_o}\right)$

p local static pressure, pounds per square inch

p_o free-stream static pressure, pounds per square inch

q_o free-stream dynamic pressure, pounds per square inch

R Reynolds number based on mean geometric chord of wing

S wing plan-form area including that blanketed by the fuselage, square inches

S_T wing area of triangular wing having the same leading-edge length and sweep angle as the given swept wing, square inches

t/c maximum thickness of streamwise wing section

V_o free-stream velocity, feet per second

X streamwise distance from midchord of mean aerodynamic chord to center of pressure measured positive when center of pressure is ahead of midchord, inches

Y lateral coordinate, inches

$\Lambda_{L.E.}$ sweep angle of leading edge, degrees

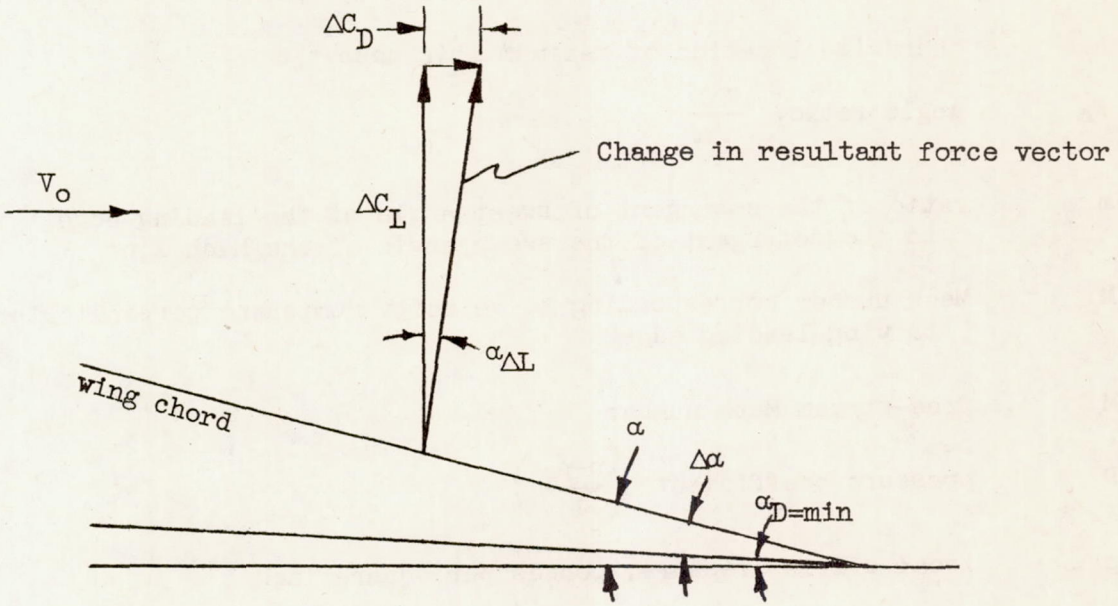

α angle of attack, radians (unless otherwise specified)

$\Delta\alpha$ change in angle of attack from value for minimum drag, radians (unless otherwise specified)

$\alpha_{\Delta L}$ rearward inclination of the change in resultant force corresponding to the change in lift coefficient ΔC_L, radians (unless otherwise specified)

Subscripts

$L=0$ value at zero lift

$D=min$ value at minimum drag

exp	experimental value
theo	theoretical value
opt	value at optimum lift coefficient
l	value for lower (parabolic) range of drag curve

EXPERIMENTAL CONSIDERATIONS

Wind Tunnel and Balance

The investigation was performed in the Ames 1- by 3-foot supersonic wind tunnel No. 1 which was fitted temporarily with a fixed nozzle designed for a Mach number of 1.5 providing a 1- by 2-1/2-foot test section. The wind tunnel, electric strain-gage balance, and instrumentation are described in detail in references 5 and 6. A cutaway drawing of the strain-gage balance is shown in figure 1.

Models and Supports

Photographs of the wings and fuselage used in the investigation are shown in figures 2 and 3 and the design dimensions of the basic configuration are shown in figure 4. The fuselage and wings were constructed of steel and no attempt was made to fair in their junctures. In addition to the design setting of 63° the model was constructed so that leading-edge settings of 57.0°, 60.4°, 67.0°, and 69.9° could also be tested. The setting of 60.4° locates the trailing edge at the Mach angle corresponding to a Mach number of 1.53 and those of 57.0° and 69.9° were the limits of the range attainable. For purposes of brevity, the wing-fuselage configurations will be designated by the letters WF followed by a two-digit number giving the leading-edge sweep angle to the nearest whole degree. Thus the basic wing-fuselage configuration is designated WF-63.

The streamwise airfoil section of the wing of WF-63 is an NACA 64A006. A section having a rounded leading edge was employed in an attempt to realize the leading-edge suction force predicted by theory when the wing leading edge is swept within the Mach cone. Because it was desirable to have the wing thickness-chord ratio as small as possible to minimize the pressure drag and still obtain a wing that was structurally practical, the limitations of present-day

construction were considered. Since at the present time the minimum depth at the root is approximately one-fifteenth the spar distance from the root to the centroid of panel area, the ratio of 1:13.6 obtained with the wing of WF-63 indicates a slightly greater wing thickness was employed than was required by this structural criterion.

To obtain the four additional leading-edge sweep settings, the half-wings were rotated about the midpoint of the root chord. Thus, increasing the sweep angle resulted in a decrease in streamwise thickness-chord ratio, a decrease in aspect ratio, and a rearward movement of the position of maximum streamwise section thickness. (The structural criterion was not violated in any case.) Table I shows the variation of the geometric parameters affected by rotating the wing panels.

The fuselage shape used has been determined by Haack, reference 7, to have the minimum pressure drag for a given length and volume assuming closure at the tail as is shown by the broken lines in figure 4. The model fuselage shape, however, had a base to permit installation on the balance sting, the area of the base being large enough to shield the sting shroud. In order to obtain a variation of the incidence angle of the fuselage on the sting, the model fuselage was constructed in two parts as is shown in figure 2. The fuselage used for obtaining force data had 4° incidence to the sting axis so that with the balance beam travel of ±5° indicated in figure 1, the total angle-of-attack range was from -1° to 9°. A photograph of the model mounted in the tunnel prior to a force test is shown in figure 3. Plan-form schlieren and liquid-film photographs were obtained during special tests with the model rotated 90° from the position shown in figure 3. The balance beam was set at zero angle of attack for these tests and the desired lift coefficients were obtained by selection of the afterbody with the required incidence angle.

To obtain a fuselage for the fuselage-alone force tests, the fuselage wing slots were filled and the metal formed in a manner that gave circular sections normal to the longitudinal axis.

Test Methods

The methods used for determining the aerodynamic forces on the model were the same as those of reference 5. Measurements were made of lift, drag, and pitching moment.

The liquid-film technique employed in reference 5 was used to determine the nature of the boundary-layer flow on the model surfaces

at all sweepback settings for zero lift and at selected lift coefficients. The technique, adapted for supersonic flow from a method developed by Grey (reference 8) depends primarily upon the difference in the rates of evaporation within laminar and turbulent flow areas. In addition to indicating areas of laminar and turbulent flow as in reference 5, where the patterns obtained were photographed outside of the tunnel after the test was completed, the photographs obtained in the present tests while the tunnel was operating indicate the location of the line of laminar separation and in some instances the direction of the boundary-layer flow.

Schlieren plan-form photographs were taken during all tests in which liquid-film patterns were recorded. It was determined during a specific test that the presence of the liquid film and fluid ridges therein did not alter the shock-wave pattern or aerodynamic forces on the model.

Corrections and Precision

The effect of support interference was taken into account in the manner described in reference 5. Liquid-film studies showed that the boundary layer was turbulent over the rear of the fuselage and remained unseparated up to the fuselage base. Reference 9 indicates that the effect of the support system on the pressures on the model will then be confined to the base pressure. The base pressure was measured in each test and the drag force was corrected for the difference between the test and the static pressure of the free stream at the fuselage base. Drag corrections for the longitudinal pressure gradient of the stream were calculated for the wings and fuselage and were found to be negligible.

All experimental lift curves have been plotted against the angle of attack of the root chord and no attempt has been made to determine the average angle of attack due to wing twist under load. The variation of the wing twist with angle of attack was found to be approximately linear for the basic configuration WF-63 and corresponded to 0.3° washout at the optimum lift coefficient.

The accuracy of the experimental data is the same as that determined in reference 5 since the experimental technique and equipment were essentially the same. However, the sting moment gage was changed prior to the present investigation and the improvement in construction eliminated the discrepancies noted near zero lift in the previous tests. More experimental points were also obtained in the present investigation to permit more accurate fairing of the data.

THEORETICAL CONSIDERATIONS

Aerodynamic Characteristics

The theoretical characteristics of the wings in this investigation have been determined on the basis of linear theory or approximate linear theory insofar as practicable. Existing theory permits the determination, exclusive of the effects of viscosity, of the lift and pitching moment and the drag due to lift for four of the wings. For the most highly swept plan form (WF–70) the Mach lines from the root trailing edge intersect the wing leading edge and the solution for this case was not attempted.

Since by symmetry, the values of lift and moment at zero angle of attack are zero, and the drag at zero angle of attack is a minimum, the longitudinal aerodynamic characteristics can be defined by the lift–curve slope $dC_L/d\alpha$, the moment–curve slope dC_m/dC_L, the the minimum drag coefficient $C_{D_{min}}$, and the drag–rise factor $(\Delta C_D/\Delta C_L)^2$.

Slopes of lift and pitching–moment curves.– The linear theory as applied by Cohen (reference 10) has been used to determine the slopes of the lift and pitching–moment curves. The moment curves obtained by the linear theory are linear; whereas the experimental curves were found in all cases to be nonlinear. Hence, the lengthy calculations to obtain the moment–curve slopes were carried out only for WF–63, the basic configuration. The theory of reference 10 is exact to the order of the linear theory for the wings of WF–57 and WF–60. The values obtained for the wings of WF–63 and WF–67 must be considered approximate since the solution for the pressures in the area between the root trailing–edge Mach line and the trailing edge is obtained by a method which involves certain minor violations of the boundary conditions. It is believed, however, that these calculated slopes are close to the values that would be obtained from the exact linear theory solution.

Minimum drag coefficient.– For convenience in the analysis, the minimum drag coefficients have been treated in terms of their components, the thickness and friction drag of the wings, and the thickness and friction drag of the fuselage. It should be noted that in determining the skin–friction coefficients the low–speed skin–friction coefficients have been used. Because it was not possible to determine quantitatively the skin–friction coefficient within observed separated flow regions, this component of the wing drag was obtained by assuming completely laminar flow at a Reynolds

number of 0.62 million.

The values of the estimated minimum drag coefficients for the wings must be considered approximate since no solution was available for the determination of the thickness drag of wings with rounded leading edges. The theoretical values used in this analysis were obtained from the curves of reference 11, which consider variations in leading-edge sweep angle, aspect ratio, taper ratio, thickness-chord ratio, and Mach number for wings having a double-wedge profile with maximum thickness at midchord. Although this airfoil section has a sharp leading edge, the experimental results of references 5 and 12 indicate that there is little, if any, change in wing drag associated with the rounding of a sharp leading-edge section on a wing swept within the Mach cone. Probably a more important difference, between the actual wing sections and that used in the theoretical analysis, is the distribution of wing section thickness. However, this deviation will not alter the qualitative variation of wing pressure drag with changes in sweep.

The thickness drag coefficient for the fuselage alone has been determined by the method of characteristics (reference 13) and in each case has been based on the wing area of the particular configuration. Liquid-film results indicated that behind the point of intersection of the wing leading edge the fuselage boundary layer was turbulent. To account for this, an approximation of 40-percent laminar and 60-percent turbulent flow was used to obtain the total friction drag coefficient using equation (5) of reference 14. This equation assumes that the turbulent boundary layer over the rear of the fuselage is the same as would be obtained if the flow over the entire fuselage were turbulent.

The components of the drag obtained in the manner discussed previously, have been tabulated below for four of the configurations. For the most highly swept-wing configuration it was not possible to determine the wing-thickness drag coefficient from the curves of reference 11. The effects of wing-fuselage interference have been neglected.

Configuration	WF-57	WF-60	WF-63	WF-67
Wing-thickness drag	0.0150	0.0078	0.0047	0.0026
Wing-friction drag	.0034	.0034	.0034	.0034
Fuselage thickness drag	.0015	.0015	.0016	.0016
Fuselage friction drag	.0034	.0034	.0036	.0036
Total	0.0233	0.0161	0.0133	0.0112

Drag due to lift.– The theoretical drag–rise factor as given in reference 5 is

$$\frac{\Delta C_D}{(\Delta C_L)^2} = \frac{k_a}{dC_L/d\alpha} \tag{1}$$

where k_a defines the rearward inclination of the resultant force on the flat lifting surface as a fraction of the angle of attack. As was discussed in references 1 and 5, the theoretical value of k_a equals one when the lifting wing has a supersonic leading edge. However, for a lifting wing with a subsonic leading edge, suction pressures develop near the leading edge (see fig. 5, which is the qualitative lifting pressure distribution determined from the results of Stewart, reference 15) reducing the rearward inclination of the resultant force and the theoretical value of k_a to less than one.

The amount of theoretical leading–edge suction for a wing of the present investigation is the same as that for a swept–back triangle having the same leading edges. Based on this consideration, the following expression obtained from the results of reference 1 may be used to determine k_a.

$$k_a = 1 - \frac{S_T}{S} \frac{\pi m \sqrt{1-m^2}}{\sqrt{M_o^2-1}\,(dC_L/d\alpha)E^2} \tag{2}$$

In this equation, S_T is the area of the equivalent triangle and E is the complete elliptic integral of the second kind with the modulus $\sqrt{1-m^2}$. Values of $\Delta C_D/(\Delta C_L)^2$ were obtained by substituting equation (2) into equation (1).

Maximum lift–drag ratio and optimum lift coefficient.– The theoretical maximum lift–drag ratio of the configurations in the present study may be determined from the minimum drag coefficient and the drag–rise factor. As was shown in reference 5

$$(L/D)_{max} = \frac{1}{2} \sqrt{\frac{1}{C_{D_{min}} \left[\frac{\Delta C_D}{(\Delta C_L)^2}\right]}} \tag{3}$$

and the lift coefficient for maximum lift–drag ratio is

$$C_{L_{opt}} = \sqrt{\frac{C_{D_{min}}}{\Delta C_D/(\Delta C_L)^2}} \qquad (4)$$

Thus the maximum lift–drag ratio depends equally upon the minimum drag coefficient and the drag–rise factor.

Theoretical Location of Line of Laminar Separation on Basic Configuration at Zero Lift

The pressure distribution shown in figure 6 has been used to determine the theoretical line of laminar boundary–layer separation on the wing of WF–63 at zero angle of attack. To obtain this pressure distribution, a graphical modification of the method of Jones (reference 2) was used. In applying the method, the streamwise airfoil sections were approximated as closely as possible with symmetrical 16–sided polygons; the lengths of the sides were shortest where the section curvature was the greatest. It is believed that this pressure distribution is sufficiently accurate for the prediction of the line of laminar separation although the pressures near the leading edge, because of the large wedge angle required to fit the nose radius, are uncertain. (Because of the uncertainty at the leading edge, this pressure field was not used in the previously discussed determination of the wing pressure drag.)

The heavy solid line shown on the half–wing plan form in figure 6 is the theoretical line of laminar boundary–layer separation which was determined from the theoretical pressure distributions on sections normal to the wing leading edge. In reference 16, von Kármán and Millikan have shown that the point of laminar boundary–layer separation depends only upon the location of the section minimum–pressure coefficient and the rate of pressure recovery behind the minimum–pressure point. The criterion for separation developed in that reference has been used with the pressure distribution of figure 6 by applying the results of Jones (reference 17) which indicate that the characteristics of a laminar boundary layer on an oblique cylinder are determined entirely by the normal–flow Mach and Reynolds numbers. When the nomenclature of reference 16 is used, the pressure distributions normal to the wing leading edge (fig. 6) are the double–roof–profile type since the minimum–pressure location occurs

at approximately 33 percent of the normal-section chord. For this type of pressure distribution, reference 15 indicates that laminar-flow separation will occur when the kinetic energy is reduced to approximately 90 percent of its maximum value. This relationship may be written

$$\frac{1-P}{1-P_{max}} \cong 0.90 \qquad (5)$$

where P is the pressure coefficient at the point of laminar separation.

Although the theoretical considerations of reference 16 excluded the effects of compressibility, the results of reference 18 indicate that the similarities between boundary-layer flow at low and transonic speeds justify the extension of the separation criterion to the present case where the leading-edge normal flow Mach number is approximately 0.7. Therefore, equation (5) has been applied directly to the normal-section pressure distributions of figure 6 to obtain the theoretical line of laminar separation.

The foregoing discussion which assumes that the subsonic separation criterion can be used in a supersonic flow field also neglects the fact that since the wing is tapered it is not an oblique cylinder as was used in reference 17. However, the pressure distributions are approximately two-dimensional inboard from the tip Mach cones and therefore application of the method is justifiable in this region. Near the wing root the pressure field is essentially three-dimensional and is considerably affected by wing-fuselage interference so that the theoretical line is of questionable accuracy in this region.

EXPERIMENTAL RESULTS

Force Tests

The results of the force tests are presented in the usual manner as lift, drag, and pitching-moment coefficients. The following tabulation summarizes the test conditions and figure numbers in which the results are presented:

Configuration	Reynolds No. $\times 10^{-6}$	Figure No.
WF–57	0.62	7(a)
WF–60	0.62	7(b)
WF–63	0.31, 0.62, 0.84	7(c)
WF–67	0.62, 0.95	7(d)
WF–70	0.62	7(e)
Fuselage alone[1]	0.62	7(f)

Also shown on these figures are the theoretical characteristics wherever they were determined.

Figure 8 shows to a larger scale the pitching–moment data and also includes the position of the center of pressure plotted against lift coefficient. Figure 9 is a replot of the moment data in which the moments are referred to the quarter chord, rather than the mid–chord of the mean aerodynamic chord. These data may be used directly in comparing the pitching–moment characteristics with those obtained in the subsonic investigations.

Figure 10 presents cross plots of the major aerodynamic and geometric parameters against the factor m, which is the ratio of the cotangent of the sweep angle of the leading edge to the cotangent of the sweep angle of the Mach line. The variations of minimum drag coefficient, lift–curve slope, drag–rise factor, and maximum lift–drag ratio are shown in figures 10(a) through 10(d), respectively, for a Reynolds number of 0.62 million. Figure 11 presents the variations of $\Delta C_D/(\Delta C_L)^2$, k_a, and $\Delta C_L/\Delta\alpha$ with lift coefficient for WF–63 at a Reynolds number of 0.62 million.

Table II summarizes the results of the force tests for all configurations and Reynolds numbers investigated. In cases where theoretical values have been calculated they have been entered in parentheses directly below the experimental value. The theoretical results, based on linear theory, give straight-line lift and moment curves and parabolic drag curves. The experimental results, however, in all cases show nonlinear lift and moment curves and drag curves which are composed essentially of two parabolic segments that intersect at slightly less than the optimum lift coefficient. Because of these variations, two values of $dC_L/d\alpha$, $\Delta C_D/(\Delta C_L)^2$, and k_a are shown in table II for each configuration, the values being those for zero lift and for the optimum lift coefficient. The variation of these parameters with lift coefficient will be considered subsequently.

[1]Reynolds number and coefficients are based on reference lengths and area of WF–63.

Liquid-Film Tests

The results of the liquid-film tests are presented in the form of line drawings, since inconsistent lighting effects throughout the investigation resulted in a nonuniform set of test photographs. Two photographs are included, however, which show typical results obtained at zero lift and near the optimum lift coefficient. These are shown in figure 12 with the corresponding line drawings.

At zero lift (fig. 12(a)), the pattern obtained on the wing of WF-63 revealed that the boundary-layer flow on the inboard sections was laminar back to the trailing edge with the exception of a small turbulent flow area close to the body that originated at the juncture of the fuselage and wing leading edge. On the outboard sections, the boundary layer was laminar back to approximately 60 percent of the chord where the flow separated from the wing surface. The separation line is indicated in the photograph by a ridge of fluid on the surface which results from the opposing shear forces acting on the liquid film ahead of and behind the line of separation.

The lifting wing upper-surface photograph shown in figure 12(b) reveals that the laminar boundary layer separates closer to the wing leading edge than at zero lift. After separating, however, the boundary layer reattaches as a turbulent bounday layer on the inboard sections as is evidenced by the drying lines behind the separated region. The outward curvature of these lines indicated a spanwise boundary-layer flow. Outboard of the section where the line of reattached flow intersects the trailing edge of the wing, the photograph shows evidence of a secondary flow within the stalled region. On a later test run with only the bottom surface of the wing coated with liquid film, this pattern was observed to result from air flow around the trailing edge into the upper-surface separated region. In the absence of pressure-distribution studies in these tests the reason for the formation of a fluid ridge within this separated region is not immediately apparent. However, like the line of laminar separation, it must occur where there is zero surface shear in the chordwise direction.

All boundary-layer-flow drawings are of the upper wing surfaces. Since the wings were symmetrical, the patterns obtained on the bottom surfaces at zero lift were the same as those for the upper surfaces. Where upper-surface patterns are presented for the lifting wings, the lower surfaces were observed to have completely laminar boundary-layer flow.

Figure 13 presents boundary-layer-flow patterns for WF-63 showing the effect of Reynolds number at zero lift and the effect of lift at a Reynolds number of 0.62 million. Figure 14 presents the results obtained at a Reynolds number of 0.62 million for all configurations investigated.

Schlieren Photographs

Figure 15 presents two photographs of the tunnel-empty schlieren field with wind on and off, which indicate imperfections in the flow field common to all schlieren photographs presented. Figures 16 and 17 are schlieren photographs of the shock-wave patterns corresponding to the liquid-film test results shown in figures 13 and 14.

DISCUSSION

The purpose of the present investigation was to evaluate experimentally the longitudinal characteristics of a configuration which was indicated by linear theory to be capable of efficient flight near a Mach number of 1.5. Thus, the differences between experiment and theory, particularly with regard to $(L/D)_{max}$ and longitudinal stability, are of primary interest. Also of importance are the effects of both Reynolds number and sweep on maximum lift-drag ratio and longitudinal stability. In the discussion that follows, it is convenient to examine, first, the characteristics of the basic configuration WF-63 at a Reynolds number of 0.62 million and then to examine the separate effects of Reynolds number and sweep. Since, as was previously mentioned, $(L/D)_{max}$ is determined by $C_{D_{min}}$ and $\Delta C_D/(\Delta C_L)^2$ (equation (3)) and is related to $dC_L/d\alpha$, these parameters are also considered.

Characteristics of WF-63 at a Reynolds Number of 0.62 Million

Figure 7(c) shows the following discrepancies between experiment and theory:

1. The theoretical value of $(L/D)_{max}$ is 10.1; whereas the experimental value is 6.7 at a Reynolds number of 0.62 million. Comparison of the theoretical and experimental drag curves reveals that this difference is due to higher experimental values of both

minimum drag coefficient and drag due to lift.

2. The experimental value of lift-curve slope is less than that predicted by theory.

3. With regard to longitudinal stability, theory indicates a linear variation of C_m with C_L; whereas experiment shows a nonlinear variation which indicates an appreciable center-of-pressure travel.

These differences between experiment and theory are attributed to flow separation which is not considered in the linear theory but which was observed to exist on the model. The effect of this separation on the aerodynamic parameters $dC_L/d\alpha$, $C_{D_{min}}$, $\Delta C_D/(\Delta C_L)^2$, $(L/D)_{max}$, and center-of-pressure location are discussed in the sections immediately following.

Lift-curve slope.- The lift curve in figure 7(c) is composed of two linear portions that join near $C_L = 0.09$. In the lower range, the slope is 0.038 and in the range above $C_L = 0.09$, the slope increases to 0.045, both values being less than the theoretical value of 0.051 which excludes the effects of viscosity. Some insight into the effects of viscosity at a Reynolds number of 0.62 million is possible through a correlation of the lift characteristics with the boundary-layer flow as observed by liquid-film tests.

At zero lift (fig. 13(b)) on both upper and lower surfaces laminar separation occurred at approximately 60-percent chord over the outboard sections. Theory (fig. 6) predicts this separation, since the pressure recovery over the rear of these sections is sufficiently large to cause the laminar boundary layer to separate. Although theory also indicates separation should occur on the inboard sections, the experimental result at this Reynolds number revealed no such separation. This disagreement on these sections probably results in part from the departure of the flow from the two-dimensional oblique cylindrical flow assumed to exist on all sections when calculating the theoretical location of laminar separation.

As the angle of attack is increased, the separation area on the upper surface expanded to include the area on the inboard sections and the separated area on the lower surface contracted to include only the tip sections.[2] This change in boundary-layer flow was

[2]These results are based on visual observations made with the model mounted horizontally in the tunnel. Hence, it was not possible to obtain plan-form photographs of the surface flow patterns.

gradual in the range of lift coefficients below 0.09. These asymmetrical separation areas on the upper and lower surfaces effectively reduced the wing angle of attack over the sections affected and are therefore undoubtedly responsible for the low value of $dC_L/d\alpha$ obtained experimentally in this range.

Above $C_L = 0.09$, there was an abrupt change in the liquid-film pattern on the upper surface. (See figs. 13(c) and (d).) The line of laminar separation moved from approximately midchord to the region near the leading edge because of the influence of the highly adverse pressure gradients shown in figure 5. After separating, the boundary layer reattached as a turbulent flow on the inboard sections (where the pressure gradients behind the leading edge were not severely adverse). The elimination of the separation near the trailing edge on these sections increases the effective angle of attack as is indicated by the increase in lift-curve slope from 0.038 to 0.045. This change suggests that, if the flow would reattach on the tip sections, the experimental value of $dC_L/d\alpha$ would closely approach that of 0.051 predicted by the inviscid linear theory.

At $C_L = 0.21$ and 0.28 (figs. 13(c) and (d)), the line of laminar separation is very close to the leading edge except for a small length near the two-thirds semispan location. The rearward displacement of the line on these sections may be due to a localized supercritical flow based on the velocity component ($M_n = 0.69$) and wing section (similar to an NACA 0012 section) perpendicular to the wing leading edge. This condition would displace the minimum pressure point and consequently the leading-edge adverse pressure gradient region rearward as was observed in the tests of reference 19. However, no reason for the restriction of this flow alteration to only a part of the wing is apparent at the present time.

Minimum drag coefficient.- The value of $C_{D_{min}}$ obtained experimentally at a Reynolds number of 0.62 million is 0.0175 which is somewhat greater than the theoretical value of 0.0133. Several factors may contribute to this discrepancy, the most important being the increased pressure drag component included in the experimantal value which results from laminar boundary-layer separation. The previously discussed liquid-film result of figure 13(b) shows that a large separated area exists at minimum drag ($C_L = 0$). A similar condition observed in the tests of reference 20 with a swept-back-wing pressure-distribution model revealed that the pressures behind the line of separation are constant (as in subsonic flow) and more negative than indicated by theory, thereby increasing the experimental pressure drag increment. The effects of wing-fuselage interference and

wing-thickness distribution have also been neglected in the determination of the theoretical value of $C_{D_{min}}$ It is believed, however, that these factors are relatively small as compared to the effect of separation just discussed.

Drag due to lift.- The experimental drag due to lift in terms of the drag-rise factor $\Delta C_D/(\Delta C_L)^2$ has been determined from plots of $C_D-C_{D_{min}}$ as a function of $(C_L-C_{L_{D=min}})^2$ shown by curve (1) in figure 11(a) for the basic configuration. Also shown in this figure by curve (2) is the theoretical drag due to lift and by curve (3) the drag due to lift that would result if the experimental resultant force vector was perpendicular to the wing chord. Comparison of curve (1) with (2) indicates that the experimental drag due to lift is much greater than predicted by the inviscid theory. However, curves (1) and (3) indicate that the benefits of leading-edge suction are partially realized experimentally particularly in the low lift-coefficient range. This factor is apparent by considering the variations of the parameters $\Delta C_L/\Delta\alpha$ and k_a which, as shown in the section Theoretical Considerations, determine the drag due to lift. These parameters may be related by the following equation which is similar to equation (1), but does not require a linear lift curve and parabolic drag curve:

$$\frac{\Delta C_D}{(\Delta C_L)^2} = \frac{k_a}{\Delta C_L/\Delta\alpha} \tag{6}$$

Figure 11(b) shows the variations of $\Delta C_L/\Delta\alpha$ and k_a with both $(\Delta C_L)^2$ and C_L. In the range of lift coefficients from 0 to 0.09, the values of $\Delta C_L/\Delta\alpha$ and k_a are constant since, as accurately as could be determined, the lift and drag curves were linear and parabolic, respectively, in this range. At $C_L = 0.09$, where as previously discussed, the laminar boundary-layer flow separation line moved abruptly forward to the leading-edge region on the upper surface, there was an increase in the value of k_a which indicates a loss in leading-edge suction. It is noteworthy, however, that the increase in lift-curve slope and $\Delta C_L/\Delta\alpha$, because of the reattached turbulent boundary-layer flow over the rear of the wing, offsets the loss in leading-edge suction and results in a constant value of $\Delta C_D/(\Delta C_L)^2$ (fig. 11) up to approximately the optimum lift coefficient of 0.21. Above this value of lift coefficient, figure 11(a) shows an increase in drag-rise factor. Figure 11(b) indicates that this is due to increased values of k_a which probably result from the larger areas of separated

flow at both the leading and trailing edges. This change in flow is shown in figures 13(c) and (d) for lift coefficients of 0.21 and 0.28.[3] The loss of both leading-edge suction force and pressure recovery over the rear of the wing rotates the resultant force vector rearward toward the normal to the chord and hence the experimental drag-rise variation in this range approaches that of curve (3). It should be remembered, however, in comparing the calculated and experimental results, that the theoretical values of ΔC_D result purely from a consideration of the pressure drag; whereas the corresponding experimental values also include changes in friction drag which slightly increase the experimental values of k_a and $\Delta C_D/(\Delta C_L)^2$.

Maximum lift-drag ratio.- At a Reynolds number of 0.62 million the experimental value of maximum lift-drag ratio is 6.7 as compared to the theoretical value of 10.1. As is indicated by equation (3) and the values in table II, this difference is due to the higher experimental values of both $C_{D_{min}}$ and $\Delta C_D/(\Delta C_L)^2$. As was discussed in the preceding sections, the high experimental values of drag were due to flow separation. It appears, therefore, that any improvement in $(L/D)_{max}$ must come from reductions in the areas of separated flow.

Pitching-moment variation with lift coefficient.- The pitching-moment coefficients and the center-of-pressure positions for WF-63 are shown in figure 8(c). The center-of-pressure positions have been determined using enlarged plots of the moment data[4] and the following equation:

$$\frac{X}{\bar{c}} = \frac{C_m}{C_L} \tag{7}$$

[3]Although it is not immediately apparent, a close examination of figures 13(c) and (d) reveals that at the higher lift coefficient the lengths of the attached flow areas at the leading and trailing edges are appreciably reduced.

[4]The moment curves from which the center-of-pressure curves were obtained were displaced vertically by the value of the moment coefficient at zero lift which in all cases except WF-60 was small and within the limits of the experimental precision. The reason for the larger error with WF-60 was not determined. It does not, however, invalidate the variation of moment coefficient which indicates the center-of-pressure travel.

Positive values of X indicate center-of-pressure positions ahead of the transverse axis through the centroid of wing area which occurs at the 50-percent station of the mean aerodynamic chord.

The center-of-pressure travel associated with the variation of moment coefficient can be explained in terms of the changes in boundary-layer flow with lift coefficient previously discussed. Increasing the lift coefficient from $C_L = 0$ to $C_L = 0.09$ resulted in an increase in the area of separated flow on the inboard top surfaces and a decrease in area of separated flow on the outboard bottom surface. The loss of lift on the top surface occurs not far from the centroid of area, while the increase in lift on the bottom surface occurs considerably behind the centroid of area. The combined effect is to move the resultant center of pressure rearward from its location at zero lift.

Above $C_L = 0.09$ the flow on the bottom surface is entirely attached, but on the upper surface the line of laminar separation has moved close to the leading edge over most of its length. The corresponding reduction in the negative pressure peak near the leading edge has a tendency to move the center of pressure farther aft. However, as the lift coefficient increases, the separated area on outboard sections becomes progressively larger and since this loss of lift occurs behind the centroid of area, it has the effect of moving the center-of pressure forward. These opposing actions limit the maximum rearward position of the center of pressure to approximately 8 percent of the mean aerodynamic chord behind the centroid of area at a lift coefficient of 0.22. Above this lift coefficient the effect of the inboard progression of separation predominates and the center of pressure moves forward.

Effect of Reynolds Number on Longitudinal Characteristics

Because of the relatively small scale of the test model the effects of Reynolds number are important in an estimation of the characteristics of a full-scale configuration. Since similar Reynolds number effects may be expected with all configurations tested, the following discussion is primarily concerned with the changes observed with WF-63, the configuration which is a part of the general investigation at both subsonic and supersonic speeds.

Effect of Reynolds number on lift-curve slope.- The lift-curves of WF-63 are presented in figure 7(c) for Reynolds numbers of 0.31, 0.62, and 0.84 million. The values of the slopes obtained at zero lift and at the optimum lift coefficient, which are listed in table II, show that no change was observed in the test range of Reynolds numbers.

Effect of Reynolds number on minimum drag coefficient.- The measured values of minimum drag coefficient for WF-63 at Reynolds numbers of 0.31, 0.62, and 0.84 million are 0.210, 0.0175, and 0.0160, respectively. This measured decrease in $C_{D_{min}}$ results primarily from the decrease in pressure drag due to separation as is shown by the liquid-film tests results in figures 13(a) and (b) for Reynolds numbers of 0.31 and 0.62 million. (Since the decrease in skin-friction coefficient with increased Reynolds number is accompanied by an increase in wetted area, the net change in minimum drag coefficient due to these effects will probably be small.) Although the line of laminar separation is not affected on the outboard sections, there is a large reduction in the area of separated flow on the upper and lower surfaces of the inboard sections at the higher Reynolds number. The reduction in area of these separated regions is probably associated with the relatively neutral section pressure gradients (fig.6) that occur near the wing root; that is, at the higher Reynolds number, the increased energy of the boundary layer is sufficient to permit the flow to remain unseparated through the gradually rising pressure field over the rear of the wing. On the outer wing sections where the pressure recovery is more pronounced, increasing the Reynolds number has negligible effect. No liquid-film pattern was obtained at a Reynolds number of 0.84 million, but the further reduction in minimum drag coefficient to 0.0160 indicates a continuation of the changes just discussed which favorably reduces the difference between experiment and theory.

Effect of Reynolds number on drag due to lift.- As shown in the previous discussion and equation (6), the value of $\Delta C_D/(\Delta C_L)^2$ depends on the variations of $\Delta C_L/\Delta\alpha$ and k_a. Since the value of $\Delta C_L/\Delta\alpha$ is unchanged by increasing the Reynolds number, the reduction in $\Delta C_D/(\Delta C_L)^2$ is entirely due to a reduction in k_a. Near zero lift where the line of laminar separation is at approximately midchord, the reduction in k_a (table II) results from effects of Reynolds number on laminar separation similar to those discussed relative to the variation of minimum drag coefficient. The reduction in k_a with Reynolds number at lift coefficients above 0.09, as near the optimum for $(L/D)_{max}$, is probably associated with the effect of

Reynolds number on the laminar separation bubble (fig. 13(c)) near the wing leading edge. Von Doenhoff and Tetervin, reference 21, have shown at subsonic speeds that increasing the Reynolds number caused a decrease in the chordwise extent of the separated bubble. This change with increased Reynolds number resulted in an increase in the negative pressures over the wing leading edge. In the present tests the less rearward inclination of the resultant force vector with increasing Reynolds number that is shown by the reduction in $k_{a_{opt}}$ indicates a similar increase in leading-edge suction force. This effect of Reynolds number is not realized on the outboard sections where the flow does not reattach after separating near the leading edge.

The large area of the wing near the tip where the flow does not reattach indicates the detrimental effect of the adverse pressure gradient due to angle of attack (fig. 5) which exists over these sections at lift coefficients near the optimum. The accompanying increase in pressure drag associated with this pressure gradient, particularly near the leading edge when this separation occurs, is apparent by comparing the theoretical value of k_a of 0.54 for WF-63 with the values obtained near zero lift ($k_a = 0.66$) and at the optimum lift coefficient ($k_a = 0.74$) for a Reynolds number of 0.84 million. In reference 12, tests were made at the Mach number of the present study with a wing having a sharp leading edge having approximately the same length and sweep angle as WF-63 and a value of k_a of 0.79 was obtained. Comparison of this experimental result with those obtained in the present investigation of WF-63 suggests that when the line of flow separation moves near the leading edge the advantage of leading edge rounding in reducing k_a, and consequently $\Delta C_D/(\Delta C_L)^2$, is apparently lost. Thus the problem of leading-edge shape with emphasis on the reduction of the strength of the adverse pressure gradient due to angle of attack should be investigated in an attempt to maintain the maximum leading-edge suction force to the highest possible lift coefficient.

Effect of Reynolds number on maximum lift-drag ratio.- The experimental values of maximum lift-drag ratio obtained with WF-63 at Reynolds numbers of 0.31, 0.62, and 0.84 million were 5.8, 6.7, and 7.2, respectively. This increase, shown in figure 7(c) and in table II, with increasing Reynolds number results from the reductions in $C_{D_{min}}$ and $\Delta C_D/(\Delta C_L)^2$ which were discussed in the preceding sections. Although the highest experimental value obtained with this configuration is considerably less than the theoretical value of 10.1, the favorable effect of increased Reynolds number indicates

that the theoretical value should be more closely approached at Reynolds numbers somewhat above those attainable at the small scale of the present tests.

The value of the lift coefficient for maximum lift-drag ratio of 0.21 is independent of Reynolds number in the range investigated. This result is associated with the increased rate of drag rise near a lift coefficient of 0.20 which, because of the severeness of the adverse pressure gradient due to angle of attack is also independent of Reynolds number.

Effect of Reynolds number on center-of-pressure travel with lift coefficient.- The effect of increased Reynolds number in reducing the center-of-pressure travel is shown in figures 8(c) and (d) where a decrease in total travel of approximately 8 percent of the mean aerodynamic chord is indicated as a result of increasing the Reynolds number from 0.62 to 0.84 million. (The data for a Reynolds number of 0.31 million were omitted since, for this test condition, the temperature effects on the moment strain gage in combination with the relatively small moments result in excessive scatter in the plotted data.) It appears that the favorable decrease in total center-of-pressure travel with increased Reynolds number, like the increase in maximum lift-drag ratio with increased Reynolds number, is due to the decreased areas of separated flow.

Probable effects of higher Reynolds numbers.- The probable changes in the aerodynamic characteristics due to increases in Reynolds numbers above those obtained in the present study may be discussed best by considering two ranges of lift coefficient; namely, the range near zero lift where laminar separation occurs near midchord and the higher lift-coefficient range where laminar separation occurs near the wing leading edge.

In the lower range of lift coefficients, the line of laminar separation is determined by the rate of pressure recovery behind the line of minimum pressure and the energy level of the laminar boundary layer. If the boundary layer remains laminar, a continued decrease in minimum drag coefficient with increased Reynolds number may be expected for the reasons previously discussed. If, however, boundary-layer transition to turbulent flow occurs ahead of the observed laminar separation line, reference 18 indicates that the value of the right-hand side of equation (5) would become 0.5; that is, the turbulent boundary layer can theoretically withstand a pressure recovery about five times greater than that of the laminar boundary layer before separation occurs. Thus with the pressure

field shown in figure 6 and a turbulent boundary layer near midchord, no flow separation would be likely to occur on the wing of WF-63 at zero angle of attack. In tests at larger scale of a wing with approximately 63° leading-edge sweepback having a biconvex section and taper ratio of one, Frick and Boyd (reference 20) have shown, through both pressure-distribution measurements and liquid-film studies at a Reynolds number of approximately 1.8 million, that natural boundary-layer transition did occur near midchord. Hence, a similar condition may be expected with the present wing at higher Reynolds numbers. This will cause a reduction in pressure drag, but will also be accompanied by an increase in skin-friction drag. Thus an estimation of the drag of a full-scale configuration operating near zero lift at a Mach number of 1.53 depends upon a comparison of the laminar skin-friction drag and the separation drag at the test Reynolds number with the laminar and turbulent skin-friction drags of the full-scale Reynolds number. Theodorsen and Regier in reference 22 have shown that skin-friction coefficients are independent of Mach number up to at least 1.69. Therefore, at relatively high Reynolds numbers, since the laminar and turbulent skin-friction coefficients both decrease with increasing Reynolds number, it may be expected that the turbulent skin-friction coefficient will be of the same order of magnitude as the laminar skin-friction coefficient at the test Reynolds number. In this higher range of Reynolds numbers, because the separation area and associated drag will have disappeared, it is probable the drag values near the minimum will be less than that for a similar configuration in this study.

In the range of higher lift coefficients, the pressures due to angle of attack predominate and the flow-separation line in the present tests moved close to the wing leading edge. The most important effect of increasing the Reynolds number in this range of lift coefficients is that of reducing the chordwise extent of the separated bubble which exists immediately behind the line of separation. The possibility of obtaining transition in the boundary layer ahead of the line of separation and thus removing completely the separated bubble at full-scale Reynolds numbers will depend upon the length of run, leading-edge-surface condition, and the strength of the adverse pressure gradient due to the lifting pressure distribution. The reduction or disappearances of the separated area near the leading edge would probably result in an increase in the leading-edge suction and a decrease in the drag-rise factor. This decrease in the magnitude of the drag-rise factor associated with this improvement of flow in conjunction with the probable decrease in minimum drag coefficient would result in a further increase in the maximum lift-drag ratio.

Since the distance from the moment axis to the center of pressure at low lift coefficients was reduced by reducing the area of laminar separation, the reduction or disappearance of the separated flow at full-scale Reynolds numbers should result in a more rearward center-of-pressure position near zero lift. This effect is illustrated in figures 8(c) and (d) for WF-63 at Reynolds numbers of 0.62 and 0.84 million. The increase in Reynolds numbers in the higher range of lift coefficients where the line of laminar separation is close to the leading edge will decrease the extent of the laminar bubble. It is probable, therefore, that the center of pressure will have a more forward position in this lift-coefficient range with increasing Reynolds number. Thus it is to be expected that the decrease in total center-of-pressure travel with increase in Reynolds number within the range of the present investigation will be continued to higher Reynolds numbers.

Because of the high induced angles of attack on the outboard wing sections and the associated highly adverse-pressure gradients (fig. 5), full benefit of increased Reynolds number may not be achieved at lift coefficients near the optimum; that is, the flow may separate even at full-scale Reynolds numbers. A possible solution to this problem has been indicated by Jones in reference 1 where it is shown that camber and washout may be utilized at supersonic speeds to obtain a uniform lift distribution at a specific lift coefficient. Hence, the lifting pressure gradients are neutral and should not promote separation.

Effect of Sweep on Longitudinal Characteristics

The longitudinal characteristics presented in figure 7 for the various sweep angles investigated are summarized in figure 10 for purposes of discussion. These data were obtained at a constant Reynolds number of 0.62 million, the highest possible that permitted the determination of the maximum lift-drag ratio of each angle of sweep without exceeding the limits of the balance. As in the preceding sections, the effects of sweep will be considered on lift-curve slope, minimum drag coefficient, drag-rise factor, maximum lift-drag ratio, and pitching moment. Because the sweep angle was varied by rotating the wing panels about the midpoint of the root chord, there is an accompanying change in aspect ratio and thickness-chord ratio measured paralled to the plane of symmetry. These changes, it should be noted, very nearly represent the relation which must be followed in practical wing construction to maintain a given structural strength and stiffness. In the following discussion,

unless otherwise stated, the effect of sweep also includes the effects of the wing thickness and aspect ratio changes.

Effect of sweep on lift-curve slope.- Data presented in figures 7(a) through (e) show that the break in the lift curve which has been previously discussed with WF-63 is evident at all sweep angles. For this reason two values of the slope have been listed in table II which indicate the difference in slope between zero lift and the optimum lift coefficient. Also shown in table II and on the experimental plots are the theoretical values for all wings except that of WF-70. Figure 10(b) is a cross plot of $(dC_L/d\alpha)_{opt}$ and $(dC_L/d\alpha)_{theo}$ against the factor m which shows that both values decrease with increasing angles of sweep when the Mach number remains constant. The liquid-film test results give some insight as to the boundary-layer-flow changes associated with the differences between experiment and theory. The changes in boundary-layer flow on the upper surfaces of the wings near the optimum lift coefficients are shown in figure 14(b). The differences in flow pattern due to differences in lift coefficient from the optimum are relatively small and can be neglected. (See figs. 13(c) and (d).) These liquid-film patterns indicate that at the lower angles of sweep where the greatest difference between experiment and theory exists, the area of separated flow at the trailing edge is also the greatest.

Effect of sweep on minimum drag coefficient.- The theoretical and experimental variations of minimum drag coefficient with sweep are shown in figure 10(a) where it will be noted that there is a marked reduction in minimum drag coefficient with increasing sweep. The more rapid rise of $C_{D_{min}}$ obtained theoretically as m approaches a value of one (decreasing sweep) is a result of the use of a double-wedge airfoil section in the theoretical determination of the wing pressure drag; that is, at the lower angles of sweep where the ridge line of the theoretical wing is nearly sonic, the theoretical pressure drag is somewhat higher than would be obtained with the test wing section which has no abrupt change in slope at the maximum-thickness position. The variation of the theoretical pressure-drag increment for the wings as tabulated under the section Theoretical Considerations does, however, indicate that exclusive of the effect of thickness distribution just discussed the variation in wing-pressure drag almost completely accounts for the measured reduction in total minimum drag coefficient with increased sweep. The results of reference 11 show that the primary factors in reducing the wing-thickness drag are

small thickness–chord ratios, high angles of sweep, and large aspect ratios. For the present wings, where the thickness–chord ratio and aspect ratio both decrease with increased sweep (fig. 10(a)), it is probable that both the theoretical and experimental smaller rates of decrease in $C_{D_{min}}$ at the highest sweep angles are largely due to the adverse reduction in aspect ratio.

In addition to changes in wing–fuselage interference, other factors which may influence the minimum drag–coefficient variation with sweep are changes in skin friction and separation pressure drag. Figure 14(a) which presents liquid–film results at zero lift for the test configurations shows that there are small changes in the area of separated flow, particularly at the three highest angles of sweep. These results give further indication that the large variation in minimum drag coefficient with sweep is due primarily to changes in wing–thickness pressure drag rather than to changes in separation or friction drag.

Effect of sweep on drag due to lift.– As was discussed in the preceding sections, the drag curves obtained with all configurations are composed essentially of two parabolic segments which join slightly below the optimum lift coefficient. Thus the values of the drag–rise factors at the optimum lift coefficients are slightly greater than those in the lower range of lift coefficients. Both experimental values are higher than indicated by theory for the reasons previously discussed with the results of the tests of WF–63.

The experimental variation of drag–rise factor with sweep can be studied by considering the factors which determine ΔC_D at a given value of ΔC_L by use of equation (6). For a constant lift coefficient as the sweep angle is increased, the increase in ΔC_D can be attributed either to an increase in angle of attack or to a change in k_a or to changes in both. As was considered in the preceding section the lift–curve slope decreases with increasing sweep. Consequently the angle of attack for a given lift coefficient increases and contributes to an increase in ΔC_D. The variations with sweep of k_a near zero lift and at the optimum lift coefficient are shown in table II and the latter values are plotted in figure 10(c). Since the values from 57.0° to 67.0° sweep are nearly constant, this variation of k_a has little influence on the noted increase in drag–rise factor. However, above 67.0° sweep there is an abrupt increase in the value of k_a that, coupled with the decreased lift–curve slope, results in a rapid increase in the rate of drag–rise.

A general consideration of the change in liquid-film patterns of figure 14(b) agrees with the observed variation of k_a with sweep. The value of k_a will be influenced by both the leading-edge suction pressures and the amount of pressure recovery over the rear of the wing. Therefore, although the area of leading-edge attached flow and high suction pressures is reduced as the sweep angle increases up to 67.0°, the pressure recovery resulting from the increased area of reattached turbulent flow results in a nearly constant value of k_a with sweep. At the highest angle of sweep, however, all of the leading-edge suction force is lost since laminar separation occurs along the entire leading-edge length. The change in pressure distribution associated with this loss of leading-edge suction would therefore be expected to increase k_a as is shown by figure 10(c) between 67.0° and 69.9° sweep.

Effect of sweep on maximum lift-drag ratio.- Figure 10(d) shows the variation of maximum lift-drag ratio with the factor m. This curve shows that the angle of leading-edge sweep for maximum lift-drag ratio at this Mach number is near 67.0° which corresponds to a value of m equal to 0.49. The limitations of the linear theory when used with the present wings prevent a determination of the complete theoretical variation of maximum lift-drag ratio with sweep but it is noteworthy that the trend indicated by the four lowest sweep angles is similar to that obtained experimentally.

To give an indication of the relative proportions of the difference between experiment and theory due to the differences in minimum drag coefficient and drag-rise factor, an additional calculated curve is included in figure 10(d). This curve was determined using the experimental minimum drag coefficient at a Reynolds number of 0.62 million and the theoretical drag-rise factor. Thus, the difference between this curve and the experimental maximum lift-drag curve is a direct reflection of the differences in drag-rise factor. The differences between the two calculated curves is then the result of the higher experimental minimum drag-coefficient values since the drag-rise factor in both cases was taken as the theoretical value. The probable reasons for the differences between theory and experiment were discussed in the preceding sections which considered the effects of Reynolds numbers on minimum drag coefficient and drag-rise factor.

The value of m of 0.49 at which the maximum experimental lift-drag ratio occurs is close to that indicated by the theory of reference 1 for a comparable Mach number with wings having trailing edges coincident with the Mach lines. It is interesting to note

that the maximum value will occur where the rate of decrease of minimum drag coefficient is equal to the rate of increase in drag-rise factor, since at this sweep angle the rate of change in $(L/D)_{max}$ (equation (3)) is then zero. At the optimum leading-edge sweep angle (67°) for the wings of the present study, additional data were obtained at the highest possible test Reynolds number, 0.95 million, and a value of maximum lift-drag ratio of 7.4 was obtained and is indicated in figure 10(d). This increase from 7.1 at a Reynolds number of 0.62 million was found to result from decreases in both minimum drag coefficient and drag-rise factor as was noted in the discussion of the Reynolds number effect on WF-63.

The optimum lift coefficient decreases as the sweep angle increases as shown in figure 10(d). The reason for this variation is apparent from a consideration of equation (4) and the variations of $C_{D_{min}}$ and $\Delta C_D/(\Delta C_L)^2$ previously discussed.

Effect of sweep on pitching moment.- The variation of pitching-moment coefficient and center-of-pressure location are plotted in figure 8 for the positive range of lift coefficients for all configurations in the investigation. It will be noted that the variations of moment coefficient and center-of-pressure position with lift coefficient for all configurations is similar to that for WF-63 which has been previously discussed. The effect of sweep on the center-of-pressure travel is shown by a comparison of figure 8(a) for WF-57 and figure 8(f) for WF-70. For WF-57, the maximum percent travel was about 8 percent of the mean aerodynamic chord in a lift-coefficient range of 0.18, while WF-70 shows 21-percent travel in a lift-coefficient range of only 0.13. Since the actual mean aerodynamic chord length (table I) of WF-70 is greater than that of WF-57, the absolute center-of-pressure travel is even larger than that indicated by the difference in percent travel. The effect of increasing sweep on the center-of-pressure travel is thus unfavorable. Although it was expected that there might be some change in the pitching-moment characteristics as the trailing edge passed through the Mach cone for $M_o = 1.53$, no such effect was noted.

SCHLIEREN PHOTOGRAPHS

As might be expected there is a correlation between the shock-wave pattern behind the wing of each configuration and the boundary-layer flow on the wing surfaces. The location of the compression wave that exists behind the trailing edge was found to be dependent upon the area of separated flow and, therefore, also is affected by

the Reynolds number. Inspection of figures 17(a) and (b) and the corresponding liquid-film results, figures 13(a) and (b), indicates the effect of increasing the Reynolds number on the trailing shock wave of WF-63 at zero lift. This comparison shows that as the Reynolds number was increased the trailing shock wave moved closer to the trailing edge of the wing. This result is similar to that obtained with tests of bodies of revolution, reference 14, where increasing the Reynolds number moved the point of laminar separation to the rear and also moved the trailing shock wave closer to the body base. Although no appreciable rearward movement of the line of laminar separation was apparent in the present tests on the outboard wing sections, there was a decrease in the separated-flow area near the wing root which moved the inboard origin of the compression forward.

For the lifting wings, the point at which the compression wave joins the trailing edge is associated with the area of separated flow on the upper wing surface since the compression is coincident with the trailing edge on those sections with reattached turbulent boundary layer. This result is also similar to that observed in reference 14 with turbulent flow over bodies of revolution. In this case the compression wave is attached to the body base. Figures 16(b), (d), (f), (h), and (j) show that the point of intersection of the compression line and the trailing edge moves toward the tip as the sweep angle increases, this progression being the same as that shown in figure 14(b) of the extent of the turbulent flow at the trailing edges.

CONCLUSIONS

Wind-tunnel tests have been made at a Mach number of 1.53 to determine the longitudinal characteristics of a wing-fuselage combination which linear theory indicates should be capable of efficient flight (maximum lift-drag ratio of approximately 10) up to this Mach number.

1. The following conclusions were obtained from tests with the basic configuration (63° sweep of leading edge) at a Reynolds number of 0.62 million:

(a) The experimental lift-drag ratio was 6.7 as compared to 10.1 predicted by theory.

(b) The experimental total center-of-pressure travel with lift coefficient was approximately 20 percent of the mean aerodynamic chord as compared to zero travel predicted by theory.

(c) The difference between the theoretical and experimental values of maximum lift–drag ratio was found to be a result of higher values of both minimum drag coefficient and drag due to lift. These higher values of drag as well as the large experimental center–of–pressure travel were associated with relatively large areas of separated boundary–layer flow.

2. The following effects of Reynolds number were observed in tests with the 63° swept–back wing configuration:

(a) Increasing the Reynolds number to 0.84 million increased the maximum lift–drag ratio to 7.2 and reduced the total center–of–pressure travel to approximately 12 percent of the mean aerodynamic chord.

(b) The improvement in maximum lift–drag ratio resulted from decreases in both minimum drag coefficient and drag due to lift. These reductions as well as the decrease in total center–of–pressure travel with lift coefficient were attributed to reductions in the areas of separated flow as the Reynolds number was increased.

3. Tests at a Mach number of 1.53 and Reynolds number of 0.62 million of four additional sweep angles of 57.0°, 60.4°, 67.0°, and 69.9° obtained by rotating the wing panels about the midpoint of the root chord afforded the following conclusions:

(a) A maximum lift–drag ratio of 7.1 was obtained at the optimum leading–edge sweep angle of 67°. The optimum leading–edge sweep angle resulted from the opposing effects of increasing sweep in decreasing the minimum drag coefficient and in increasing the drag due to lift.

(b) The effect of sweep in decreasing the minimum drag coefficient was associated with the decrease in wing pressure drag resulting from the increased angle behind the Mach cone and the decreased streamwise thickness–chord ratio. The increase in drag due to lift with increasing sweep was primarily due to the decrease in lift–curve slope.

(c) The total center–of–pressure travel increased with increase in sweep angle but no abrupt changes in pitching–moment characteristics were found as the complement of the trailing–edge sweep angle became less than the Mach angle for a Mach number of 1.53.

(d) At the optimum leading-edge sweep angle of 67°, increasing the Reynolds number to 0.95 million resulted in a value of maximum lift-drag ratio of 7.4.

In all cases where it was possible to compare experimental values of lift, drag, and pitching moment with those calculated by the linear theory, the experimental values were, respectively, lower, higher, and less stable than those indicated by theory. These differences were due to both the low scale of test and the partial exclusion of viscous effects in the theory. The experimental and theoretical trends with sweep, however, were in good agreement.

Because of the influence of the adverse lifting pressure gradients that caused boundary-layer separation close to the leading edges of the wings in the present study, the theoretical values of maximum lift-drag ratio may not be realized at full scale with this wing. These results indicate that the use of camber and wing twist may be necessary as a means of reducing the gradient to improve the boundary-layer flow if the maximum value of lift-drag ratio is to be attained.

Ames Aeronautical Laboratory,
National Advisory Committee for Aeronautics,
Moffett Field, Calif.

REFERENCES

1. Jones, Robert T.: Estimated Lift-Drag Ratios at Supersonic Speed. NACA TN No. 1350, 1947.

2. Jones, Robert T.: Thin Oblique Airfoils at Supersonic Speed. NACA TN No. 1107, 1946.

3. McCormack, Gerald M., and Walling, Walter C.: Aerodynamic Study of a Wing-Fuselage Combination Employing a Wing Swept Back 63°.- Investigation of a Large-Scale Model at Low Speed. NACA RM No. A8D02, 1948.

4. Reynolds, Robert M., and Smith, Donald W.: Aerodynamic Study of a Wing-Fuselage Combination Employing a Wing Swept Back 63°.- Subsonic Mach and Reynolds Number Effects on the Characteristics of the Wing and on the Effectiveness of an Elevon. NACA RM No. A8D20, 1948.

5. Vincenti, Walter G., Nielsen, Jack N., and Matteson, Frederick H.: Investigation of Wing Characteristics at a Mach Number of 1.53. I – Triangular Wings of Aspect Ratio 2. NACA RM No. A7I10, 1947.

6. Van Dyke, Milton D.: Aerodynamic Characteristics Including Scale Effect of Several Wings and Bodies Alone and in Combination of a Mach Number of 1.53. NACA RM No. A6K22, 1947.

7. Haack, W.: Geschossformen Kleinsten Wellenwiderstandes Bericht 139 der Lilienthal Gesselschaft.

8. Grey, W.E.: A Simple Visual Method of Recording Boundary Layer Transition (Liquid Film) Tech. Note Aero. 1816, R.A.E. (British/U.S. Restricted), Aug. 1946.

9. Perkins, Edward W.: Experimental Investigation of the Effects of Support Interference on the Drag of Bodies of Revolution at a Mach Number of 1.5. NACA RM No. A8B05, 1948.

10. Cohen, Doris: The Theoretical Lift of Flat Swept-Back Wings at Supersonic Speeds. NACA TN No. 1555, 1948.

11. Kleissas, John: Charts of the Zero-Lift Drag of Supersonic Swept Back Wings for Various Taper Ratios. Northrop Aircraft Inc., Rep. No. GM-109, AM-51, Sept. 1947.

12. Vincenti, Walter G., Van Dyke, Milton D., and Matteson, Frederick H. Investigation of Wing Characteristics at a Mach Number of 1.53. II – Swept Wings of Taper Ratio 0.5. NACA RM No. A8E05, 1948.

13. Sauer, R.: Method of Characteristics for Three-Dimensional Axially Symmetrical Supersonic Flows. NACA TM No. 1133, 1947.

14. Chapman, Dean R., and Perkins, Edward W.: Experimental Investigation of the Effects of Viscosity on the Drag of Bodies of Revolution at a Mach Number of 1.5. NACA RM No. A7A31a, 1947.

15. Stewart, H.J.: The Lift of a Delta Wing at Supersonic Speeds. Quart. App. Math., vol. IV, no. 3, Oct. 1946, pp. 246-254.

16. von Kármán, T.H., and Millikan, C.B.: On the Theory of Laminar Boundary Layers Involving Separation. NACA Rep. No. 504, 1934.

17. Jones, Robert T.: Effect of Sweepback on Boundary Layer and Separation. NACA TN No. 1402, 1947.

18. Nitzberg, Gerald E., and Crandall, Stewart: Some Fundamental Similarities Between Boundary-Layer Flow at Transonic and Low Speeds. NACA TN No. 1623, 1948.

19. Graham, Donald J., Nitzberg, Gerald E., and Olson, Robert N.: A Systematic Investigation of Pressure Distributions at High Speeds Over Five Representative NACA Low-Drag and Conventional Airfoil Sections. NACA RM No. A7B04, 1947.

20. Frick, Charles W., and Boyd, John W.: Investigation at Supersonic Speed (M=1.53) of the Pressure Distribution Over a 63° Swept Airfoil of Biconvex Section at Zero Lift. NACA RM No. A8C22, 1948.

21. von Doenhoff, Albert E., and Tetervin, Neal: Investigation of the Variation of Lift Coefficient with Reynolds Number at a Moderate Angle of Attack on a Low-Drag Airfoil. NACA CB, Nov. 1942.

22. Theodorsen, Theodore and Regier, Arthur: Experiments on Drag of Revolving Disks, Cylinders and Streamline Rods at High Speeds. NACA Rep. No. 793, 1944.

TABLE I.- SUMMARY OF GEOMETRIC PROPERTIES OF WINGS

Configuration	$\Lambda_{L.E.}$ (deg)	A	S (sq in.)	$\frac{c_t}{c_r}$	$\bar{c}$ (in.)	$\bar{c}_g$ (in.)	t/c (percent)	h/c (percent)	M_n (M_o=1.53)	m
WF-57	57.0	4.49	7.791	0.27	1.452	1.318	6.70	38.5	0.83	0.75
WF-60	60.4	4.03	7.809	.24	1.543	1.391	6.40	39.2	.76	.66
WF-63	63.0	3.42	7.223	.25	1.615	1.455	6.00	40.0	.69	.59
WF-67	67.0	2.71	7.344	.26	1.868	1.646	5.30	41.5	.60	.49
WF-70	69.9	2.23	7.600	.25	2.078	1.845	4.65	42.6	.53	.42

Note: The aspect ratios and mean geometric chords are based on the wing area including that blanketed by the fuselage. The taper ratios and mean geometric chords neglect the slight rounding of the wing tips by assuming them to be straight lines parallel to the stream direction and tangent to the outermost true tip contour.

TABLE II.- SUMMARY OF RESULTS

Configuration	R (million)	Lift		Drag					Lift-drag ratio	
		$\left(\frac{dC_L}{d\alpha}\right)_{L=0}$ (per deg)	$\left(\frac{dC_L}{d\alpha}\right)_{opt}$ (per deg)	$C_{D_{min}}$	$\left[\frac{\Delta C_D}{(\Delta C_L)^2}\right]_1$	$\left[\frac{\Delta C_D}{(\Delta C_L)^2}\right]_{opt}$	$(k_a)_{L=0}$	$(k_a)_{opt}$	$(L/D)_{max}$	$C_{L_{opt}}$
WF-57	0.62	0.041 (.063)	0.048 (.063)	0.0220 (.0233)	0.296 (.189)	0.305 (.189)	0.70 (.68)	0.80 (.68)	6.1 (7.5)	0.25 (.35)
WF-60	.62	.040 (.057)	.047 (.057)	.0190 (.0161)	.303 (.184)	.311 (.184)	.69 (.60)	.82 (.60)	6.5 (9.2)	.23 (.30)
WF-63	.31	.038 (.051)	.045 (.051)	.0210 (*)	.336 (.185)	.354 (.185)	.77 (.54)	.90 (.54)	5.8 (*)	.21 (*)
	.62	.038 (.051)	.045 (.051)	.0175 (.0133)	.310 (.185)	.318 (.185)	.67 (.54)	.80 (.54)	6.7 (10.1)	.21 (.27)
	.84	.038 (.051)	.045 (.051)	.0160 (*)	.288 (.185)	.300 (.185)	.66 (.54)	.74 (.54)	7.2 (*)	.21 (*)
WF-67	.62	.034 (.043)	.040 (.043)	.0140 (.0112)	.347 (.196)	.354 (.196)	.67 (.48)	.77 (.48)	7.1 (10.7)	.17 (.24)
	.95	.034 (.043)	.040 (.043)	.0135 (*)	.328 (.196)	.338 (.196)	.66 (.48)	.74 (.48)	7.4 (*)	.17 (*)
WF-70	.62	.033 (*)	.034 (*)	.0125 (*)	.410 (*)	.420 (*)	.78 (*)	.94 (*)	6.9 (*)	.15 (*)

Note: For each wing the experimental value is given first and the corresponding theoretical value indicated in parentheses directly below. Where an asterisk is used, the theoretical value has not been computed.

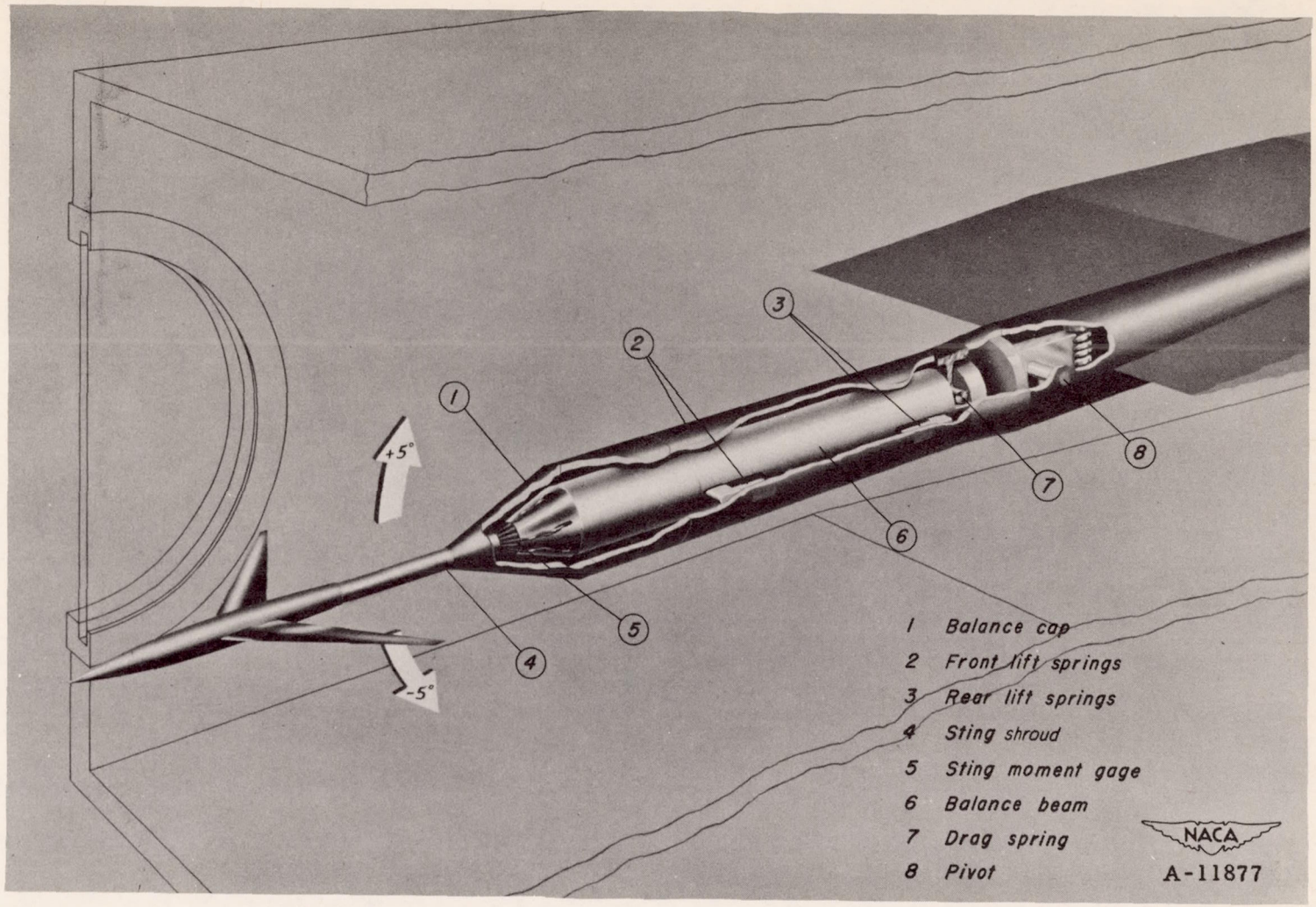

Figure 1.– Cutaway view of strain-gage balance system.

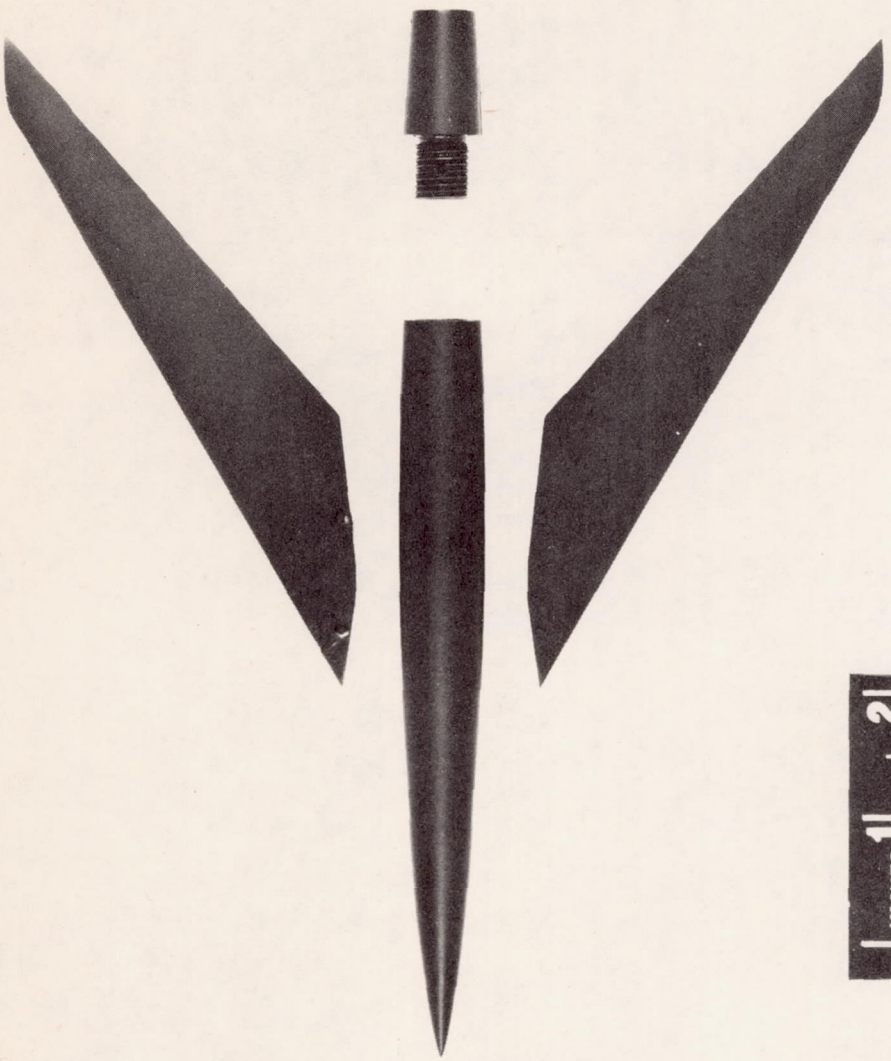

Figure 2.- Exploded view of model.

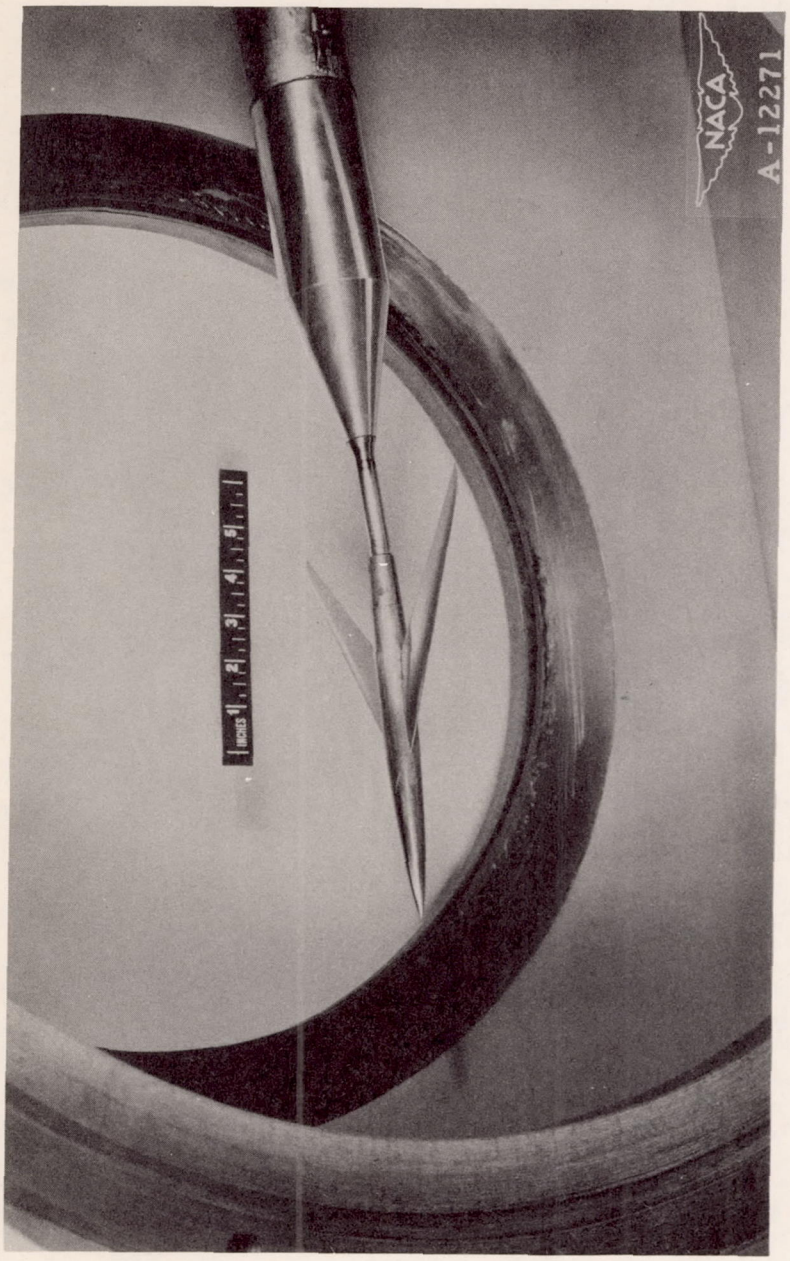

Figure 3.- Model installed in wind tunnel.

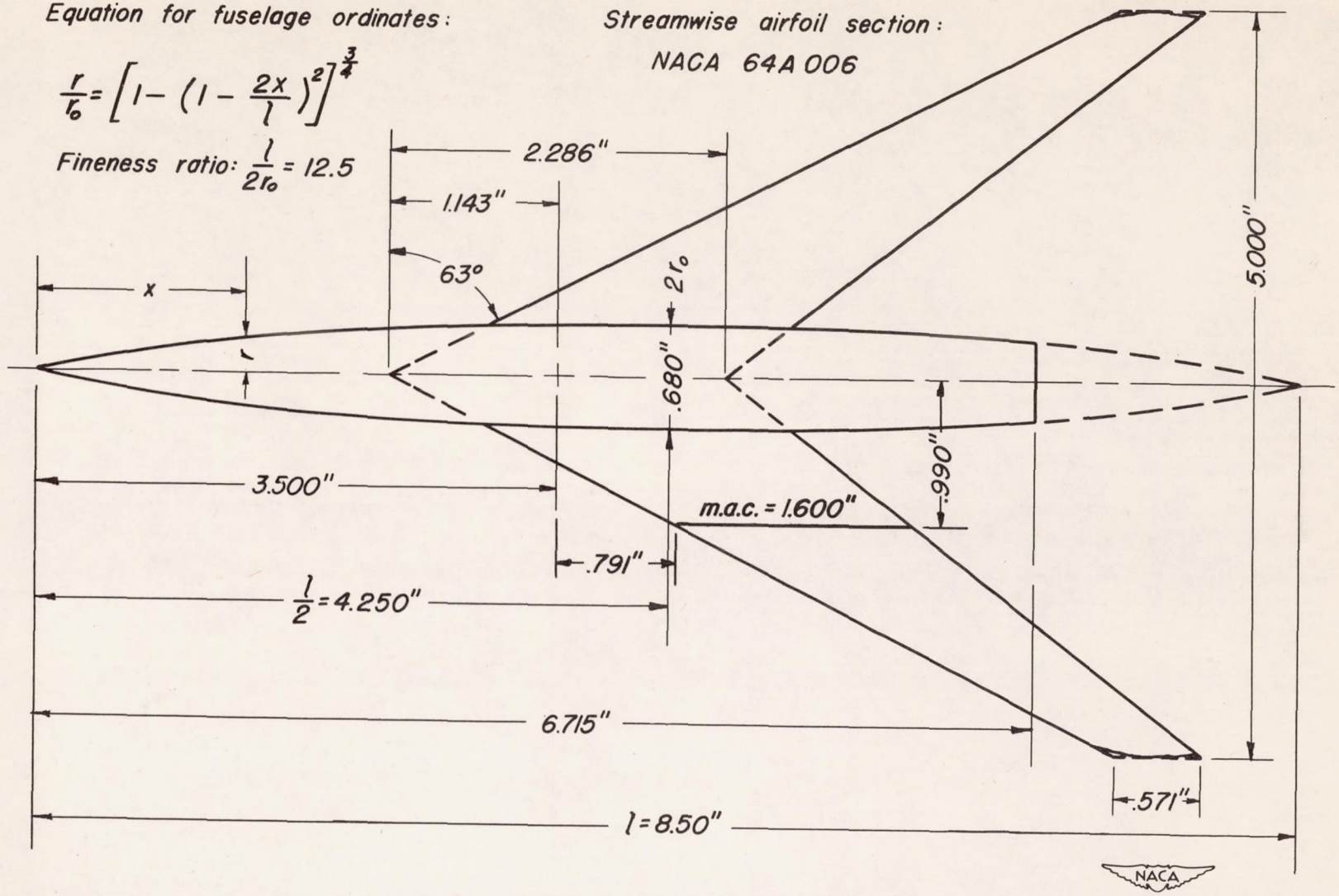

Figure 4.- Design dimensions of basic configuration, WF-63.

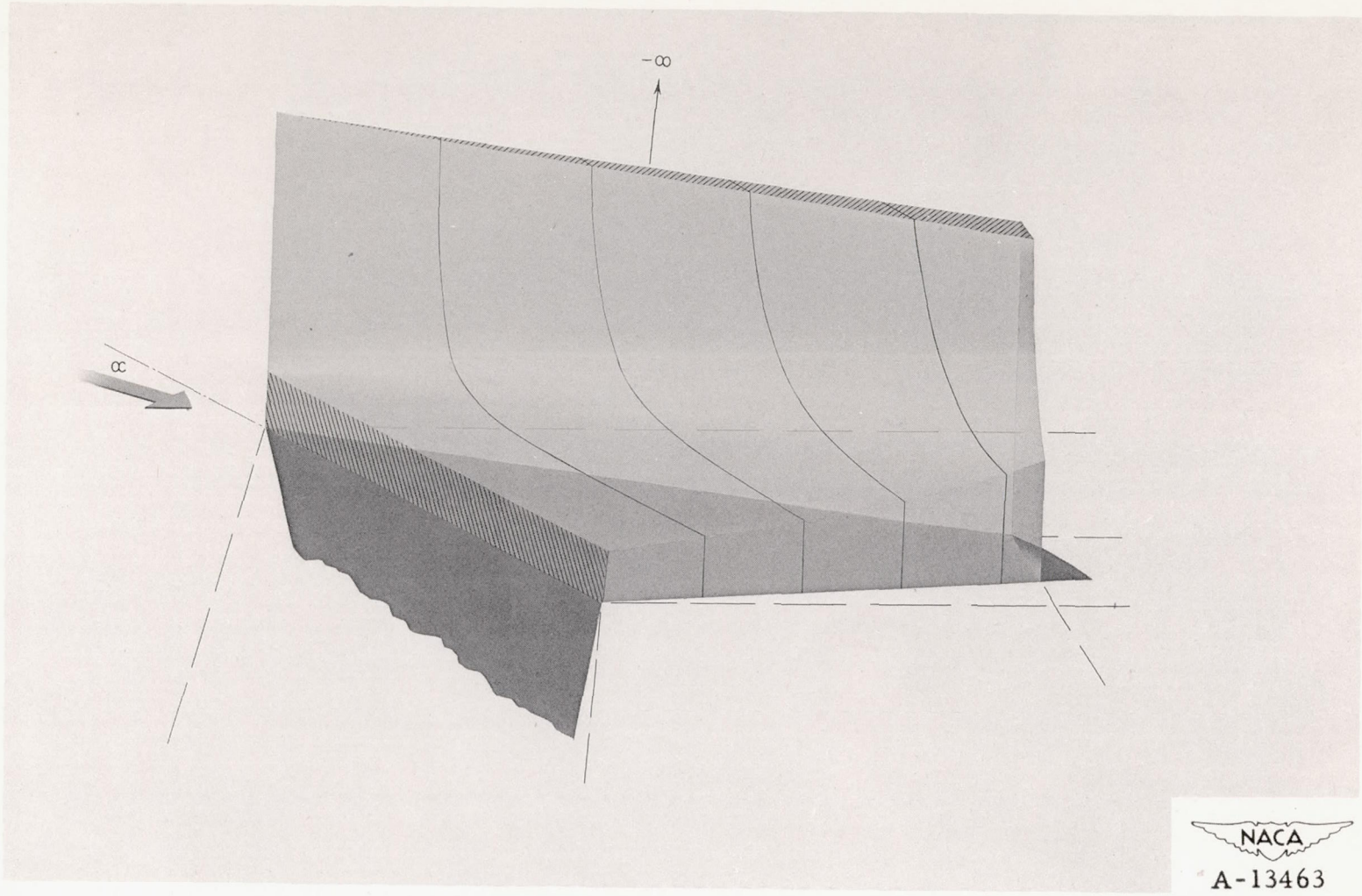

Figure 5.- Lift distribution on tapered, flat plate with leading edge swept within the Mach cone.

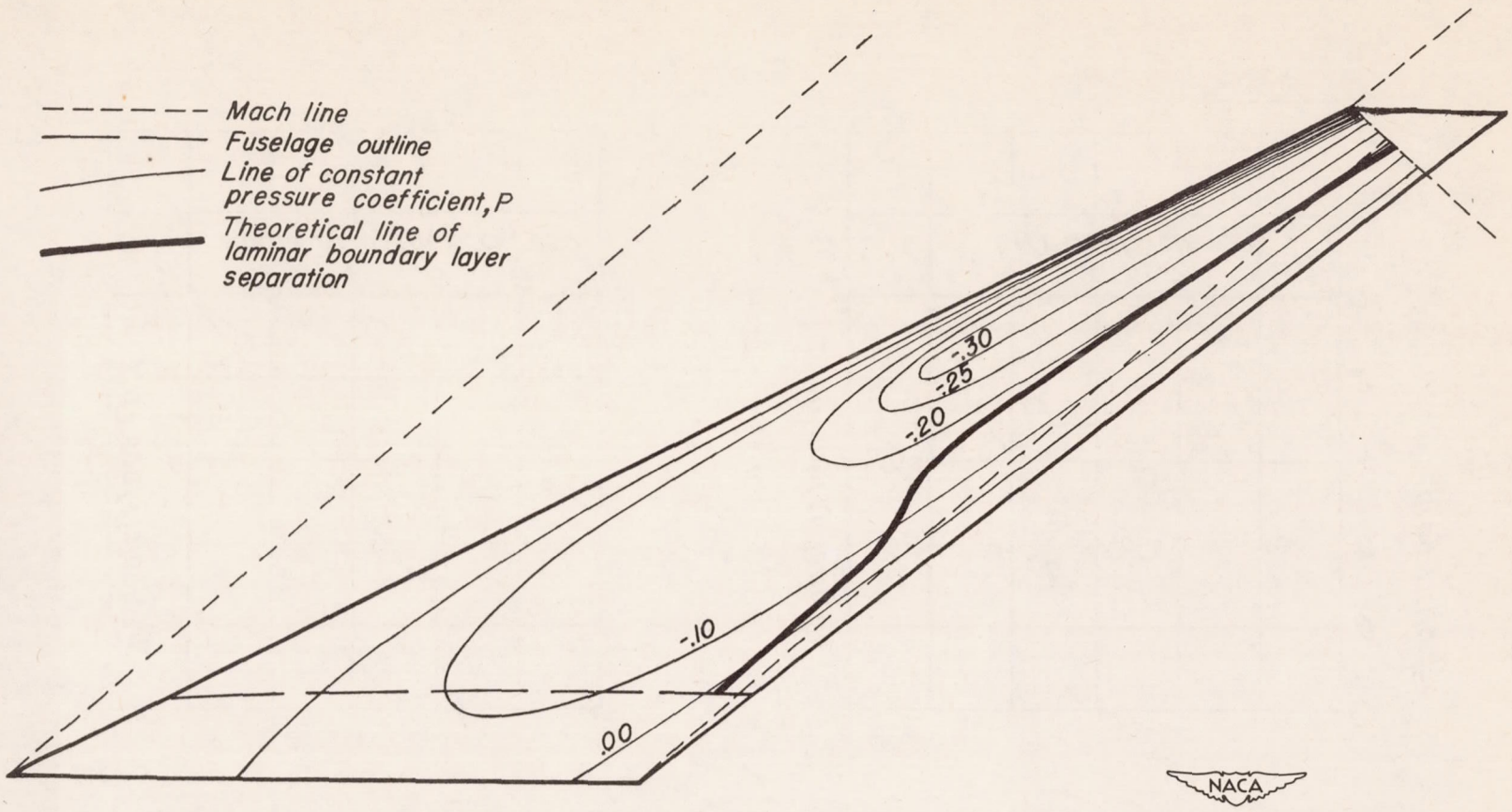

Figure 6.- Location of theoretical line of laminar boundary-layer separation on 63° swept-back wing at zero angle of attack

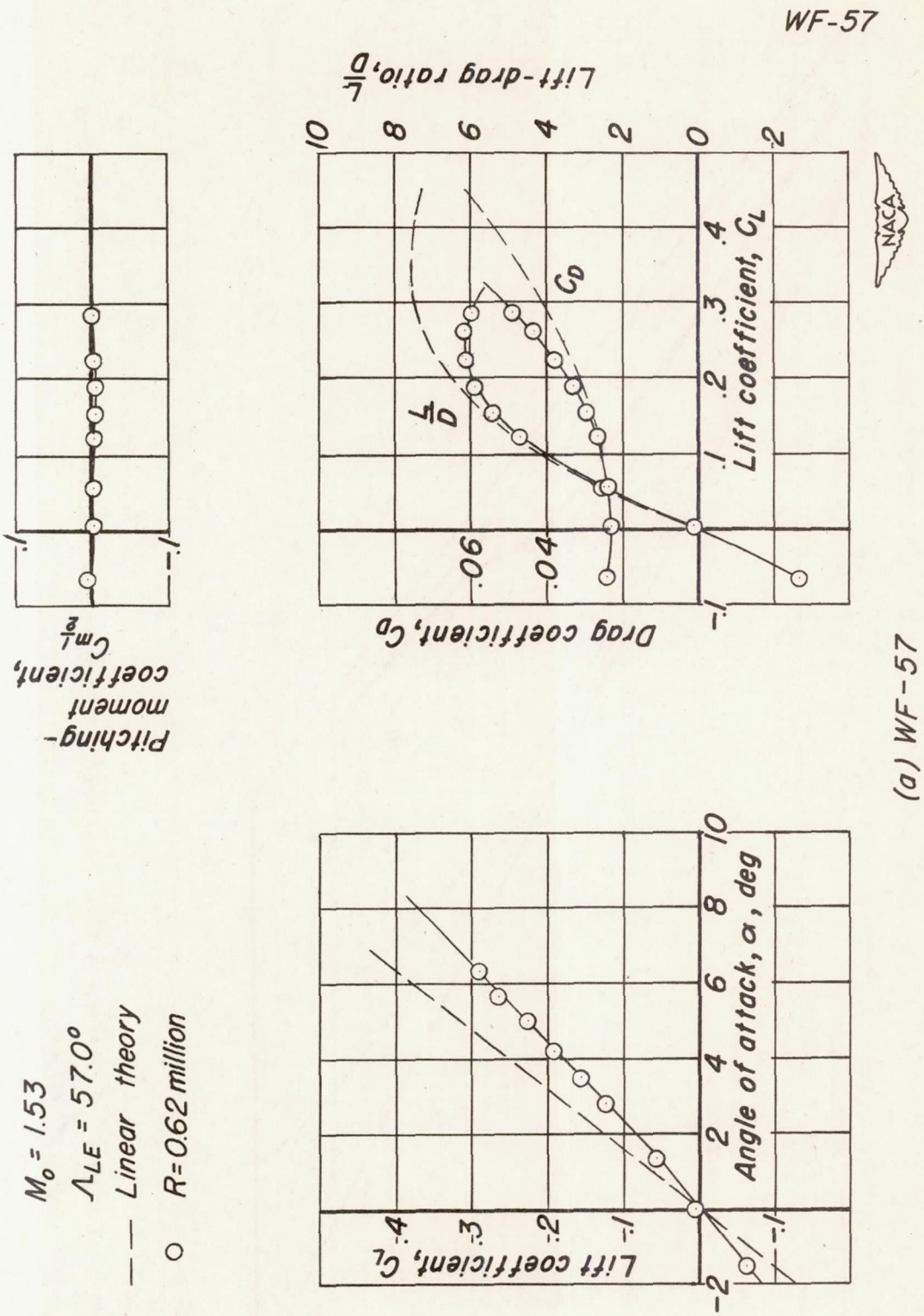

(a) WF-57

Figure 7.- Characteristics of swept-back wing and fuselage configurations.

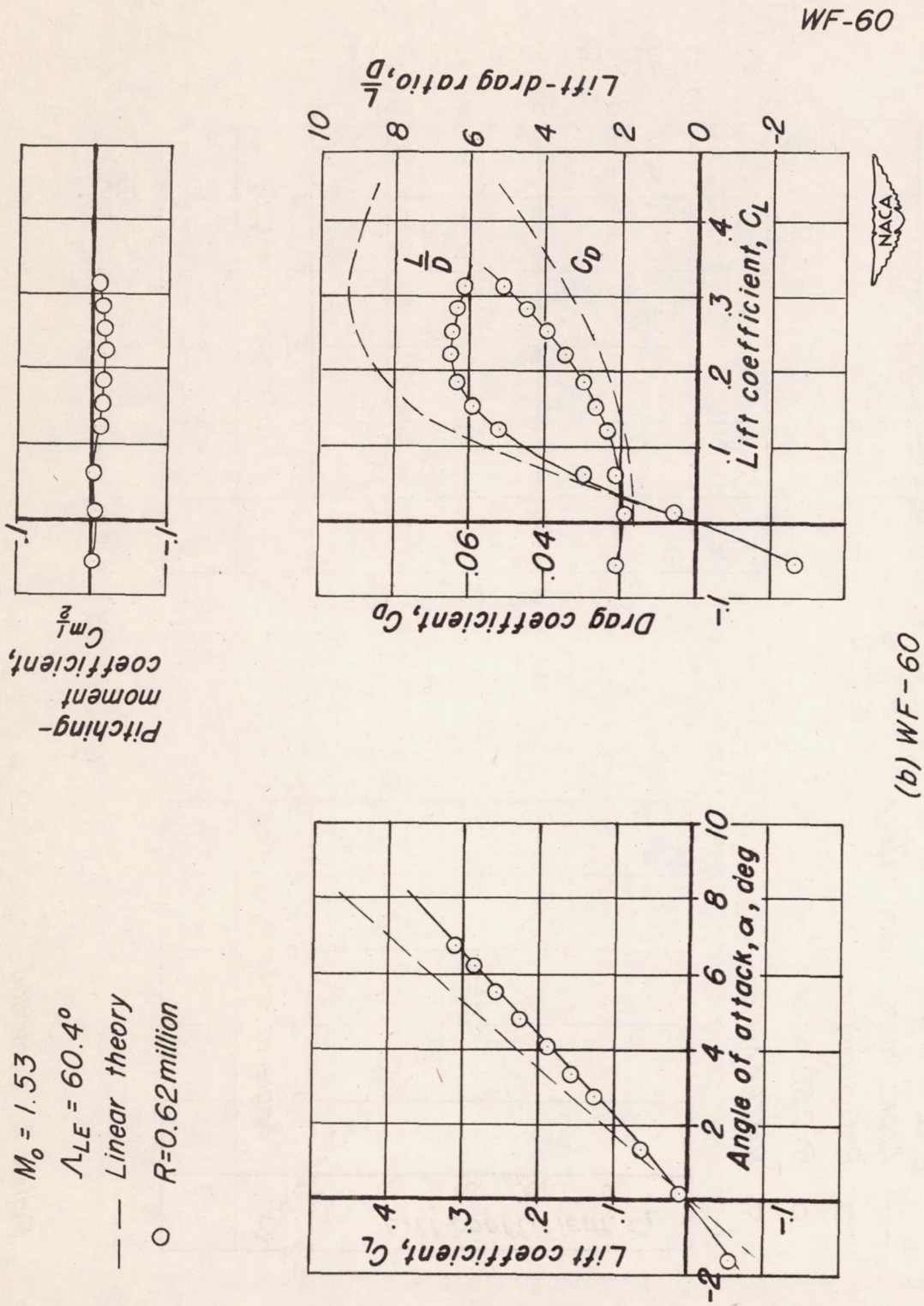

(b) WF-60

Figure 7.- Continued.

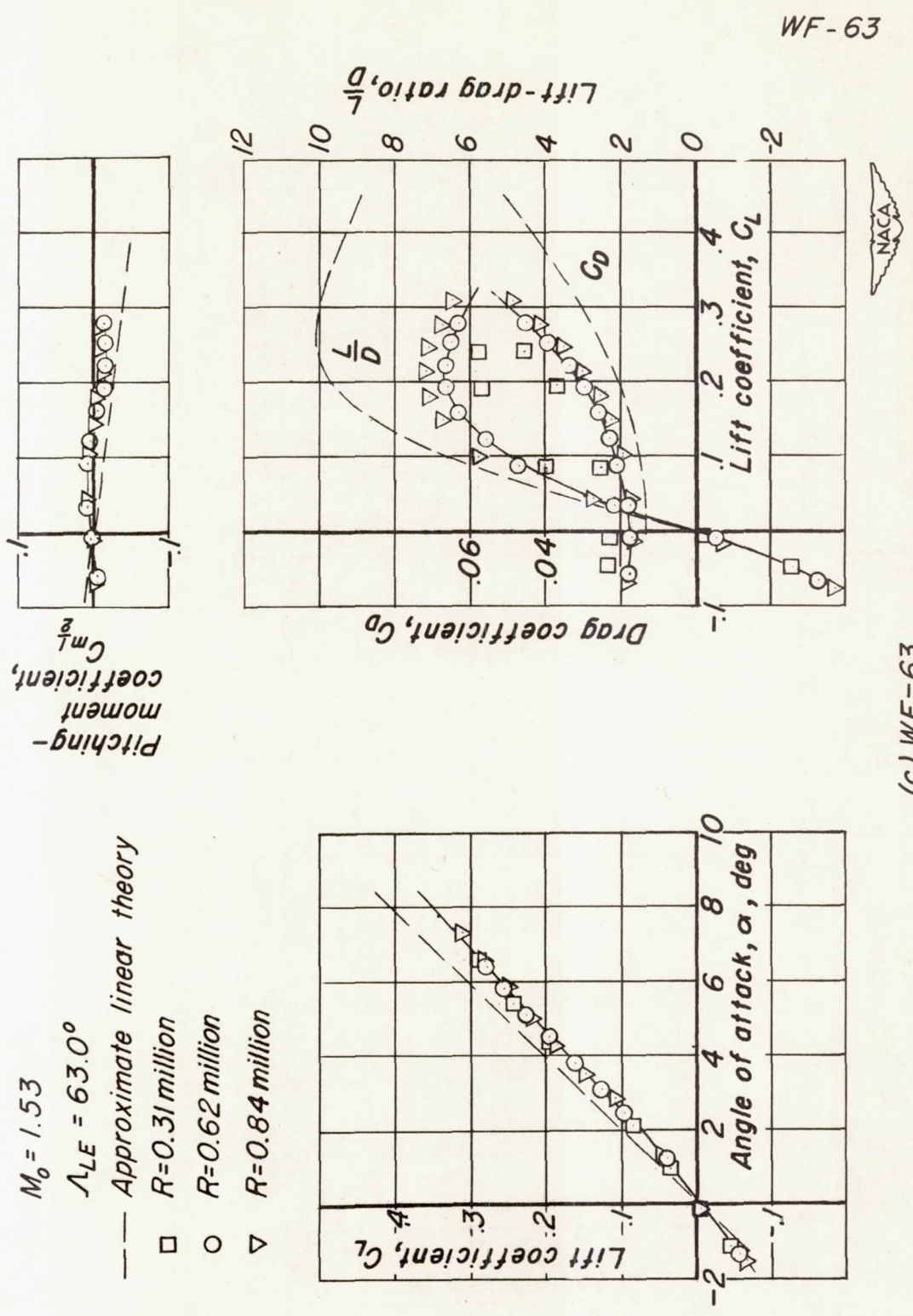

(c) WF-63

Figure 7.- Continued.

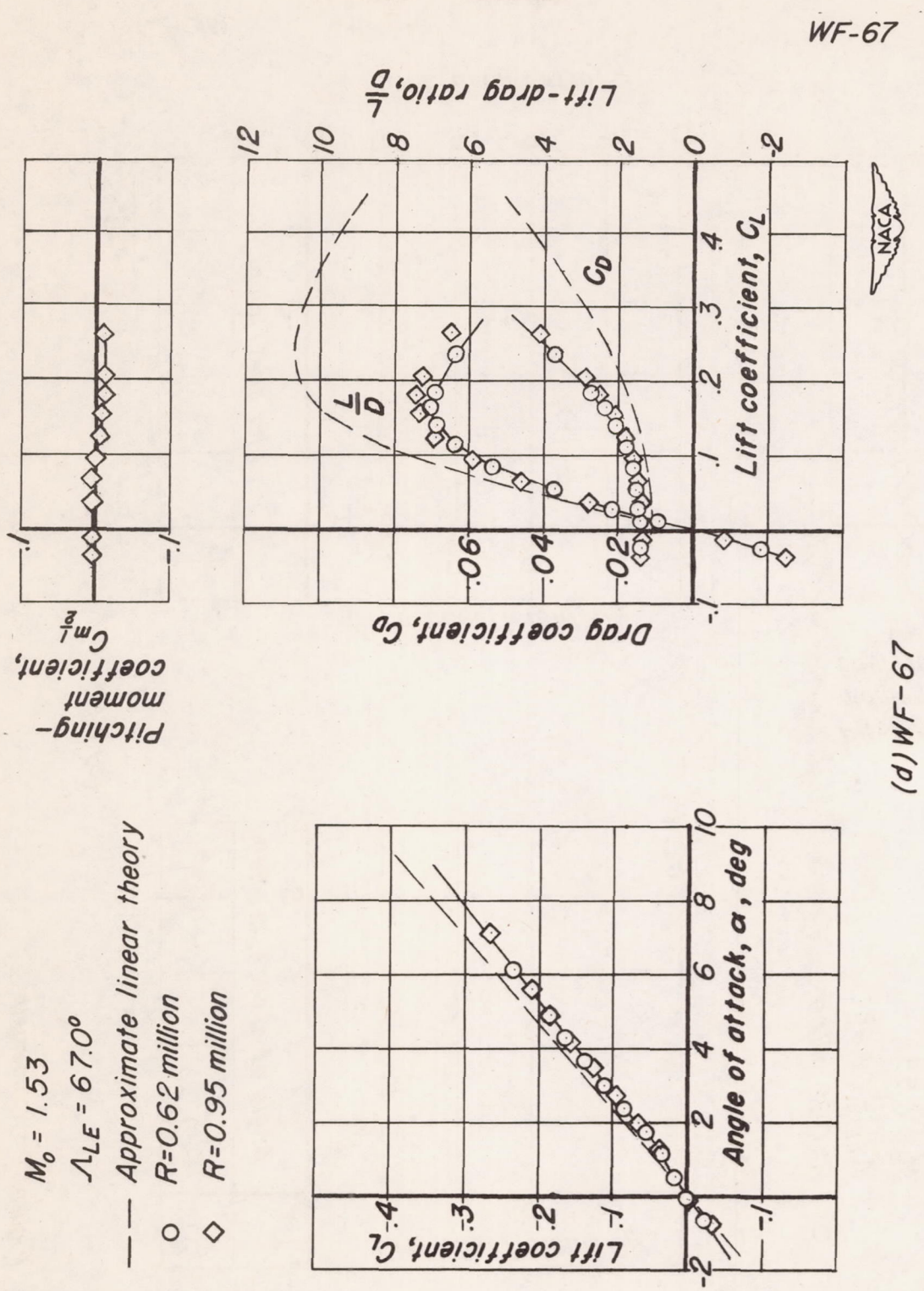

Figure 7.- Continued.

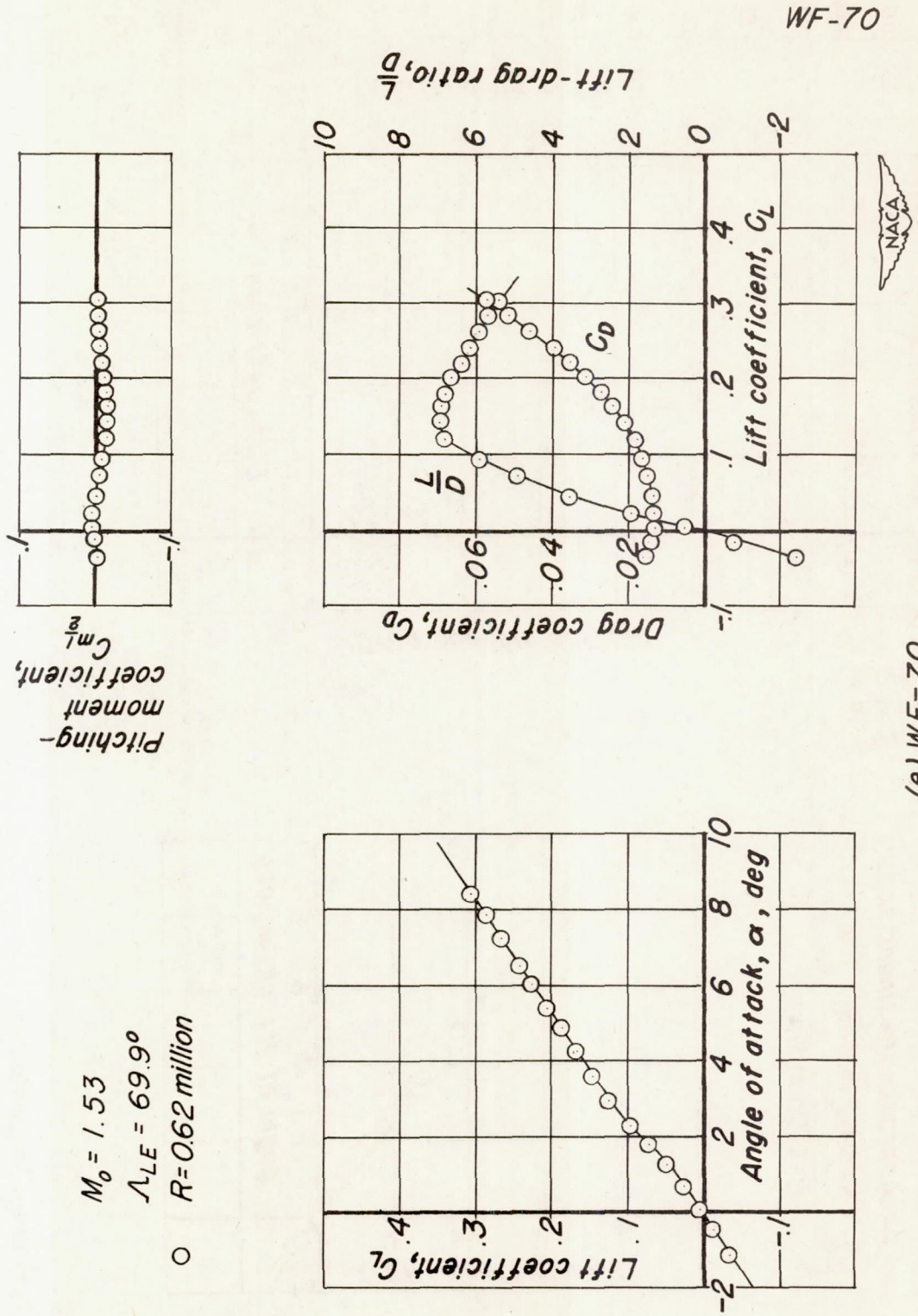

(e) WF-70

Figure 7.- Continued

(f) Fuselage alone

Figure 7.- Concluded.

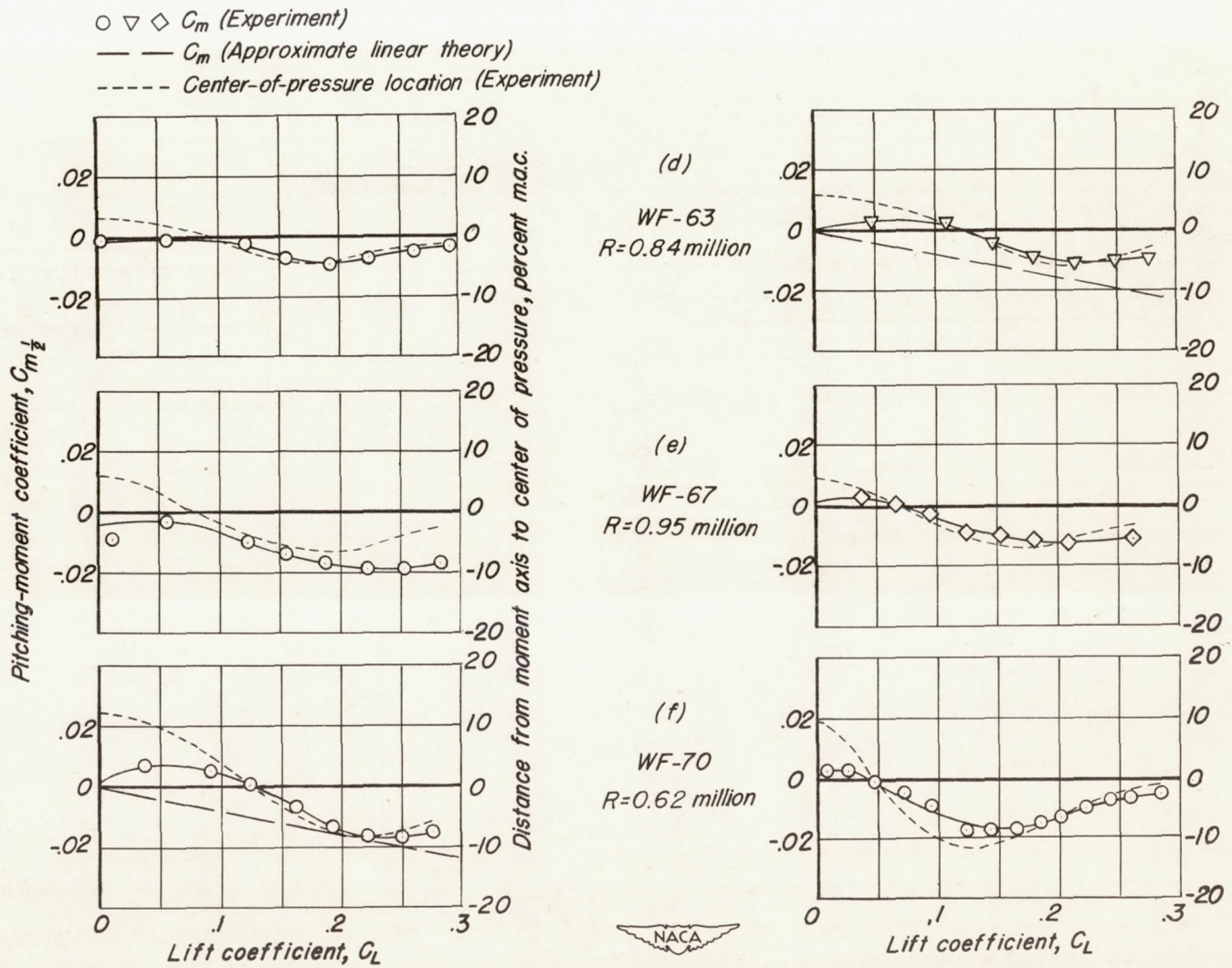

Figure 8.- Pitching-moment coefficient and center-of-pressure location variations with lift coefficient of swept-back wing and fuselage configurations. Moment reference axis at 50 percent of mean aerodynamic chord.

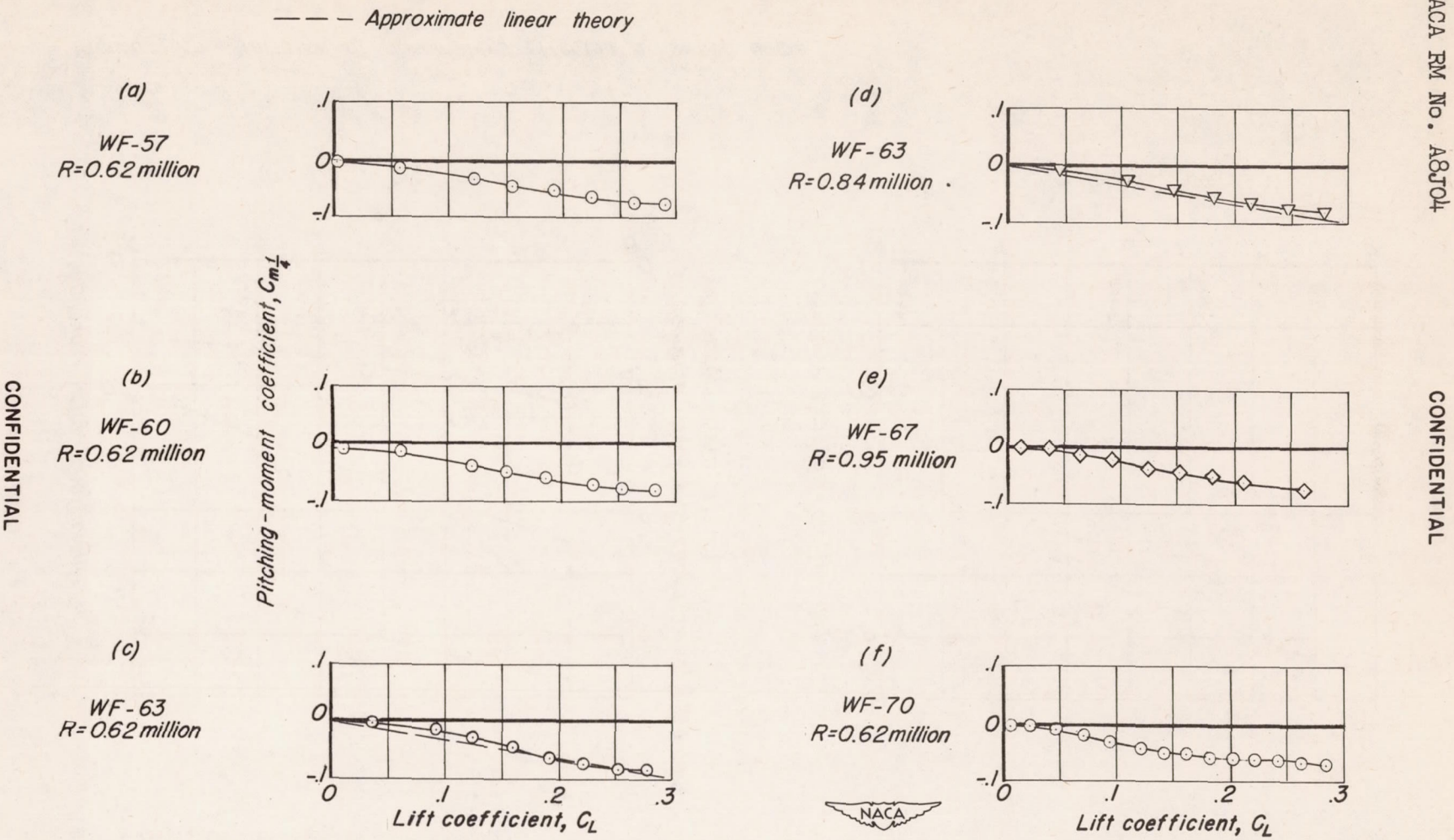

Figure 9.- Pitching-moment coefficient variations with lift coefficient of swept-back wing and fuselage configurations. Moment reference axis at 25 percent of mean aerodynamic chord.

All experimental data are for a Reynolds number of 0.62 million

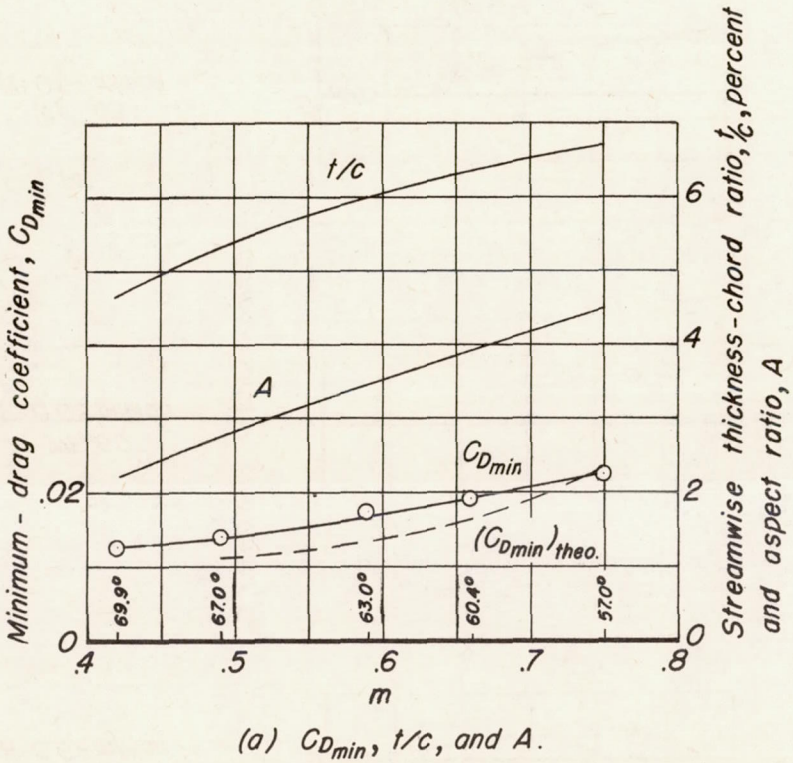

(a) $C_{D_{min}}$, t/c, and A.

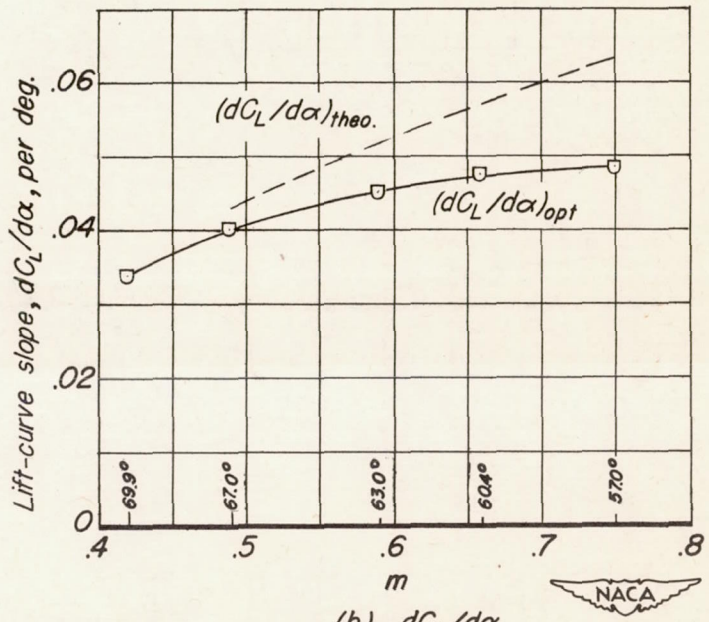

(b) $dC_L/d\alpha$

Figure 10.- Variation of parameters affected by sweep angle.

All experimental data are for a Reynolds number of 0.62 million except where noted.

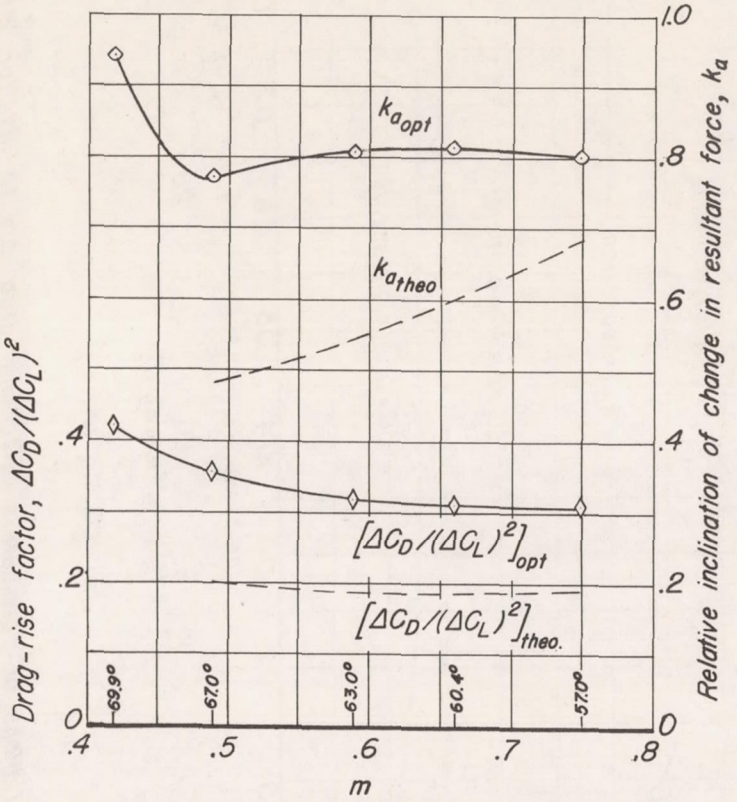

(c) $\Delta C_D/(\Delta C_L)^2$ and k_a

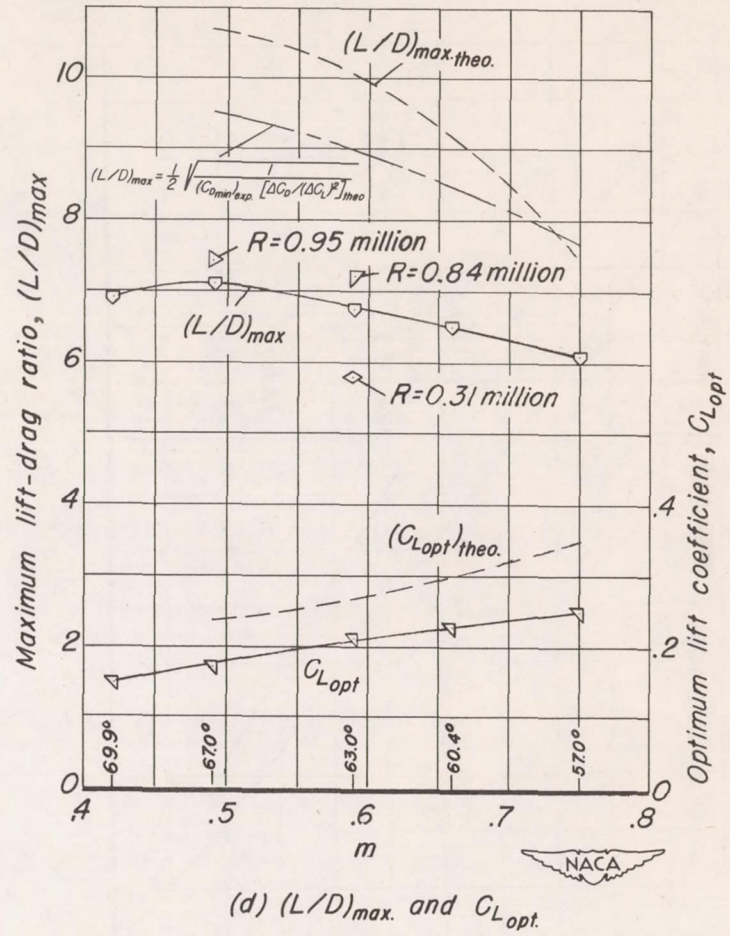

(d) $(L/D)_{max.}$ and $C_{L_{opt.}}$

Figure 10.- Concluded.

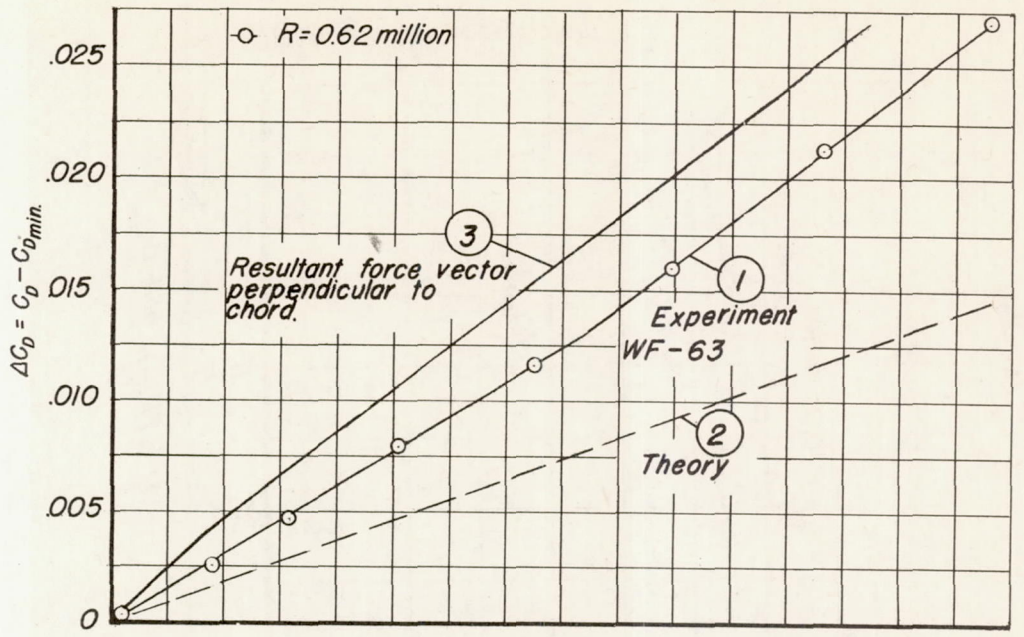

(a) $\Delta C_D/(\Delta C_L)^2$

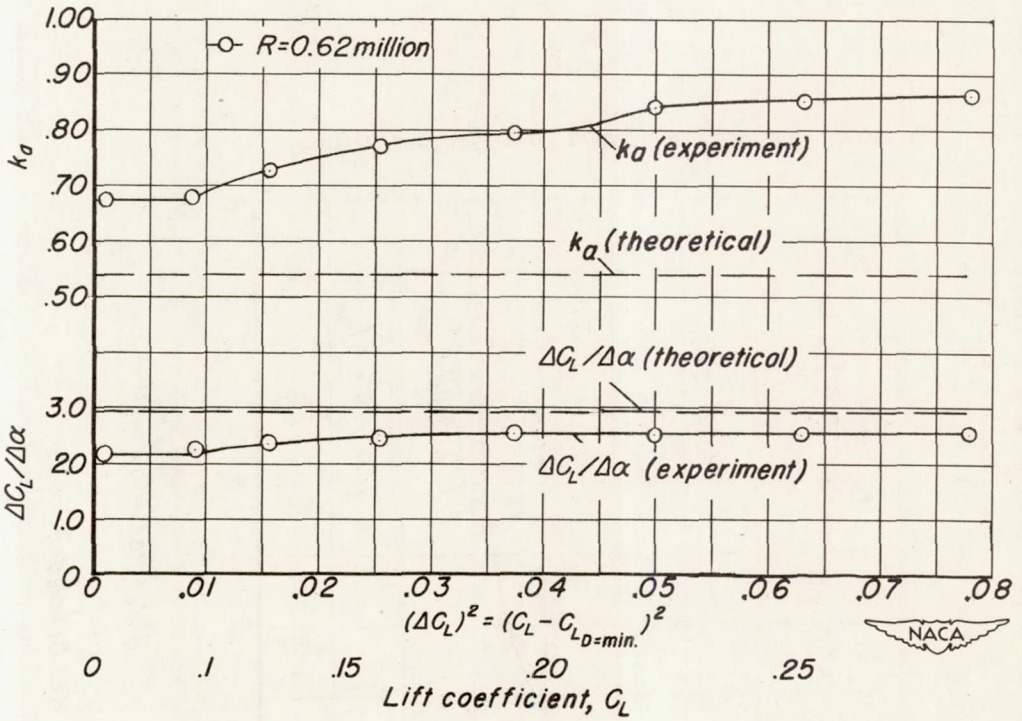

(b) $\Delta C_L/\Delta\alpha$ and k_a

Figure 11.- Variations of parameters affecting drag due to lift for WF-63.

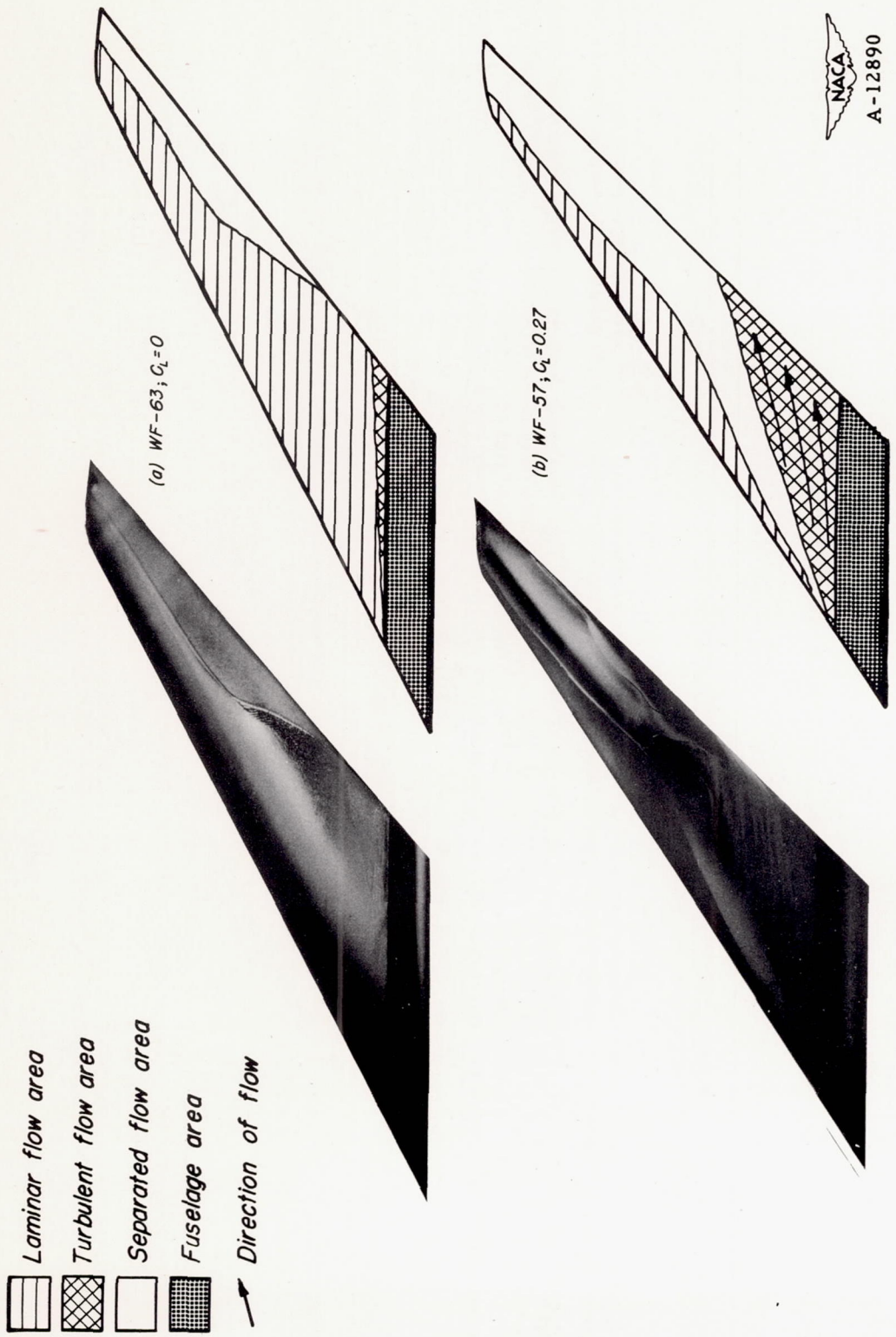

Figure 12.- Typical liquid-film test results.

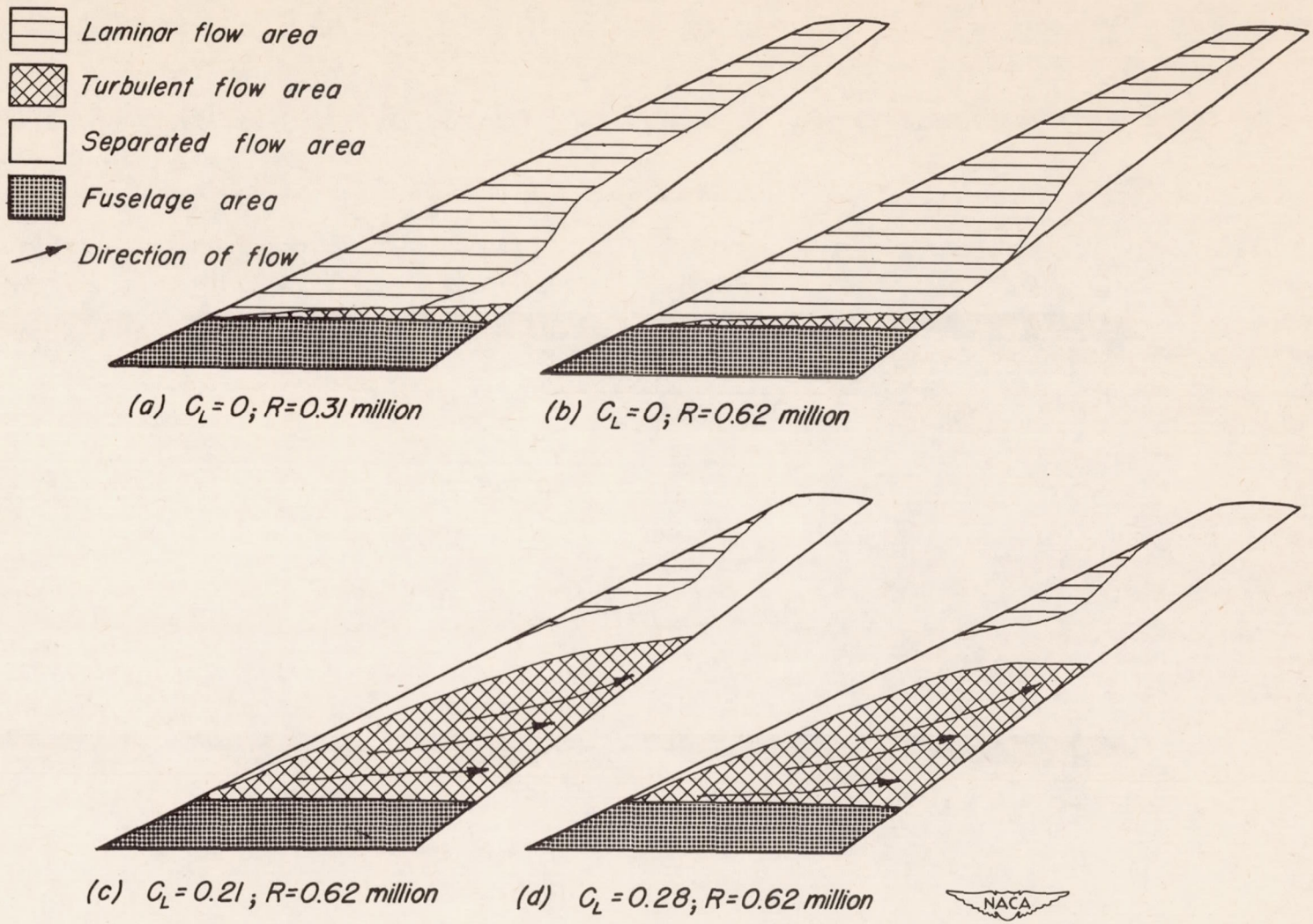

Figure 13.- Boundary-layer flow patterns on 63° swept-back wing.

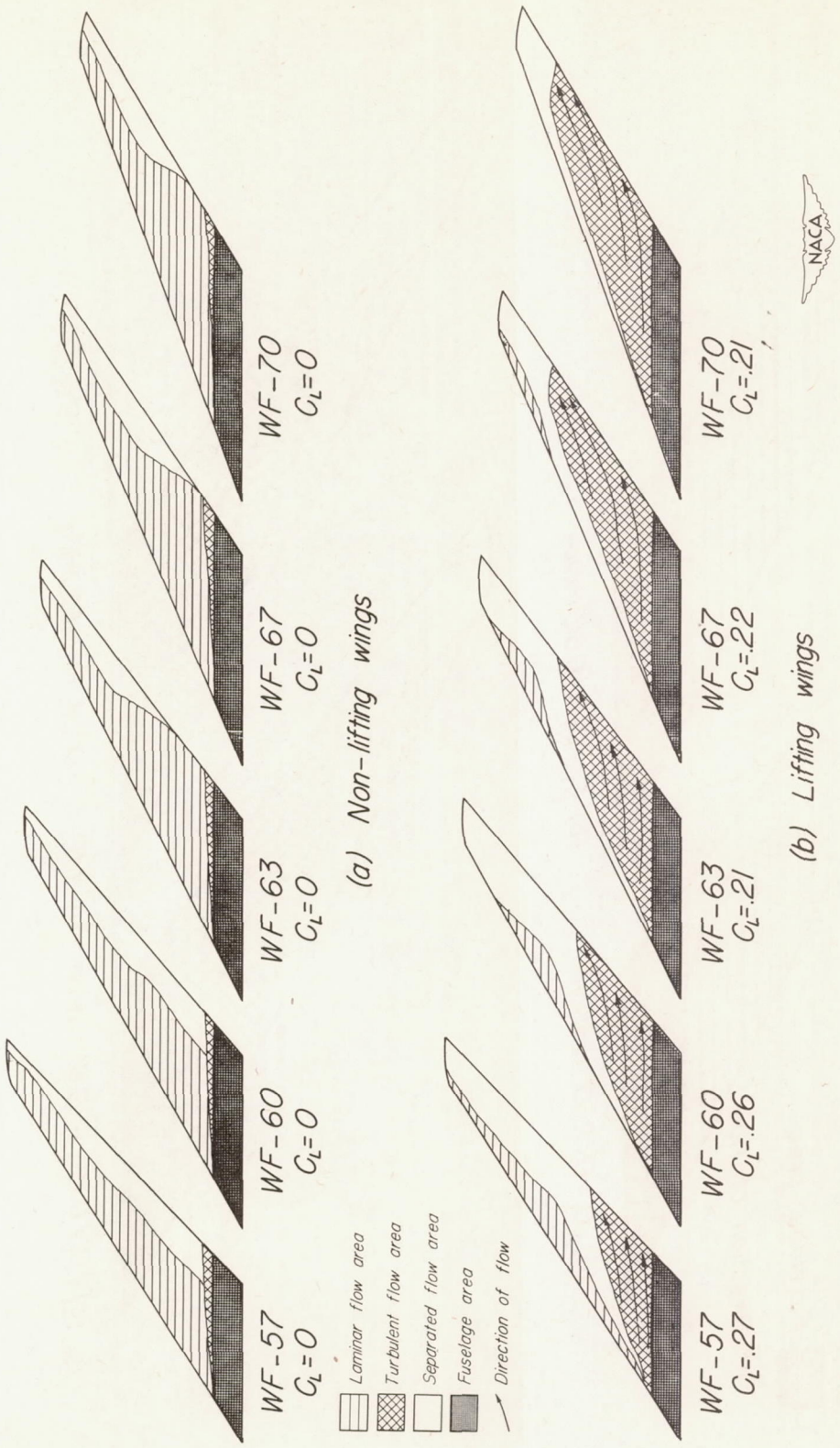

Figure 14.- Effect of sweep on boundary-layer flow at a Reynolds number of 0.62 million.

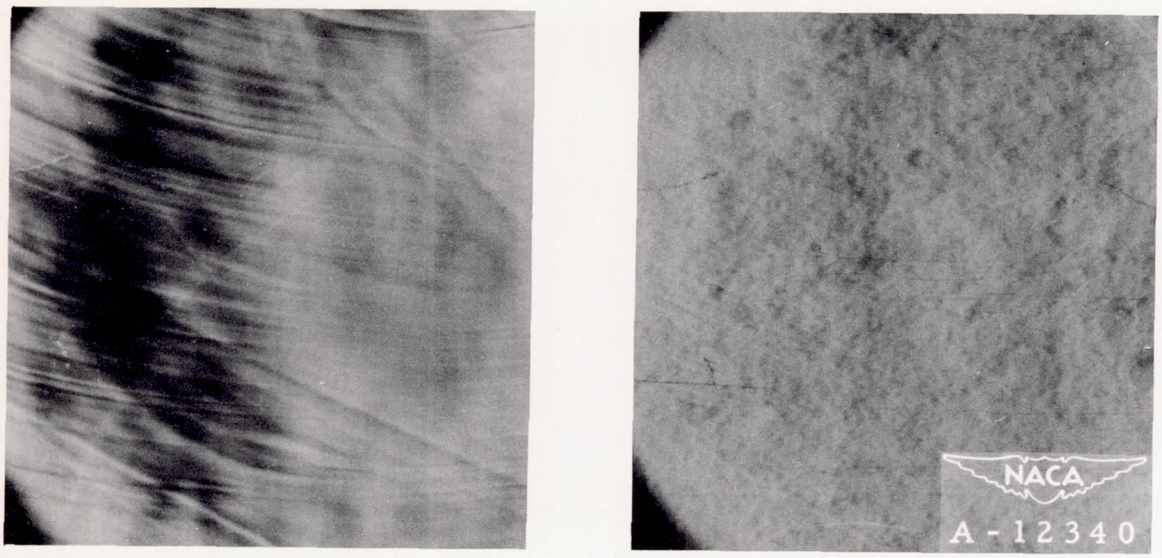

(a) Wind off.

(b) Wind on.

Figure 15.- Schlieren patterns common to all photographs.

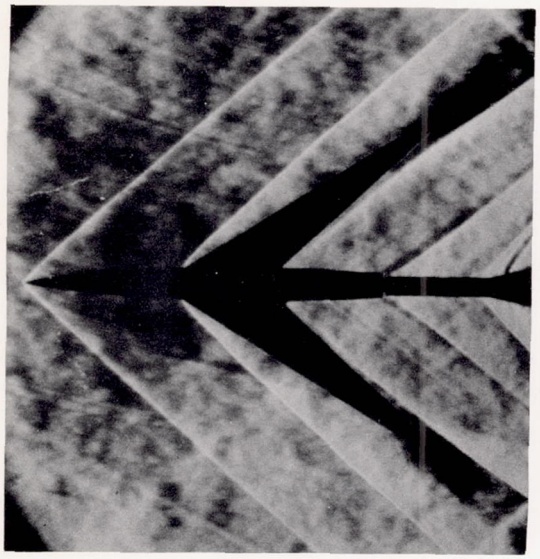

(a) WF–57; C_L, 0.

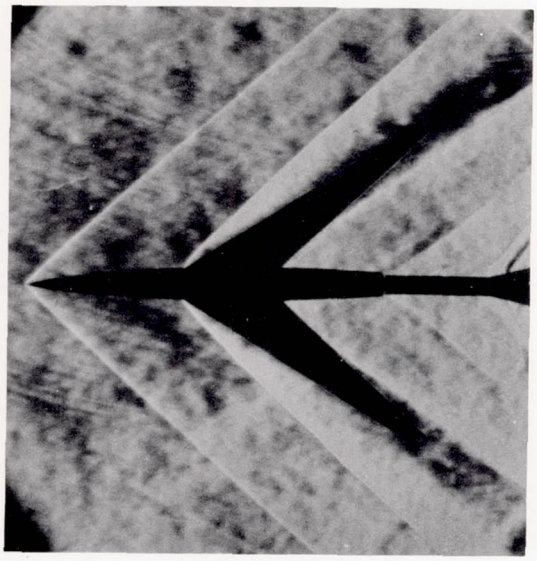

(b) WF–57; C_L, 0.27.

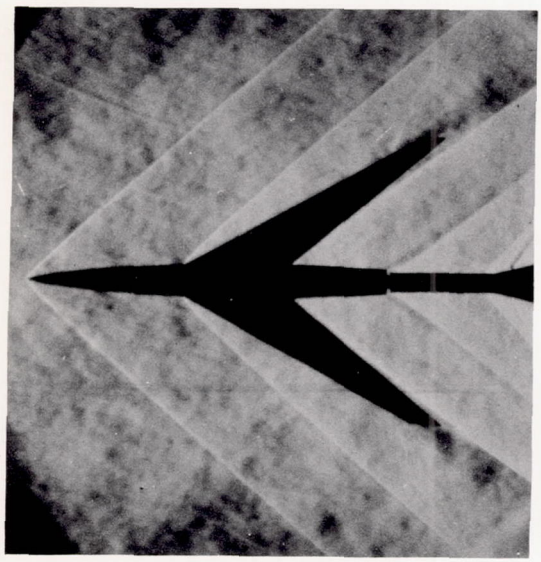

(c) WF–60; C_L, 0.

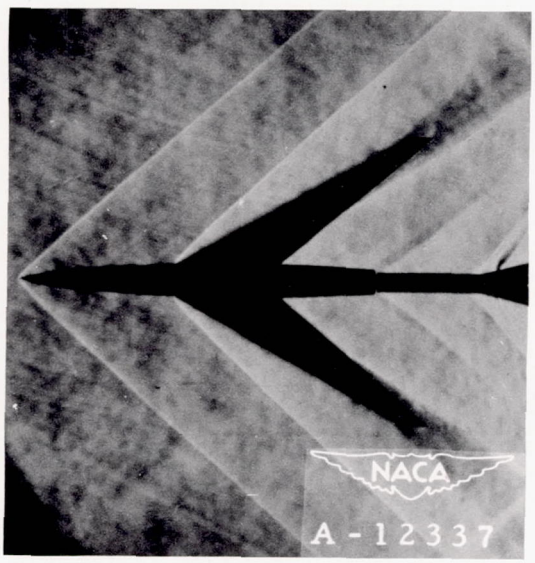

(d) WF–60; C_L, 0.26.

Figure 16.– Schlieren photographs of swept–back wing and fuselage configurations at a Reynolds number of 0.62 million.

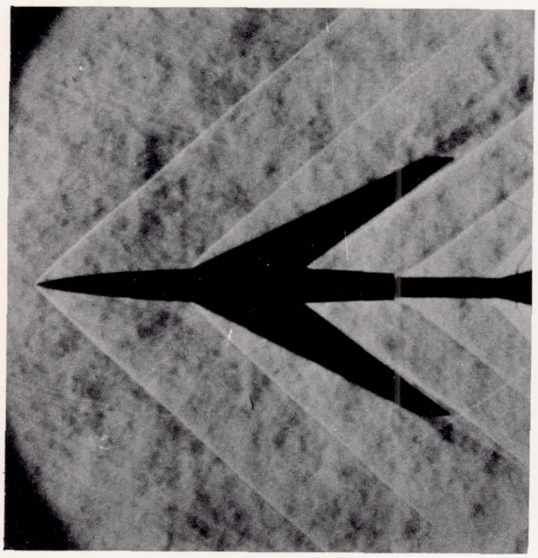

(e) WF–63; C_L, 0.

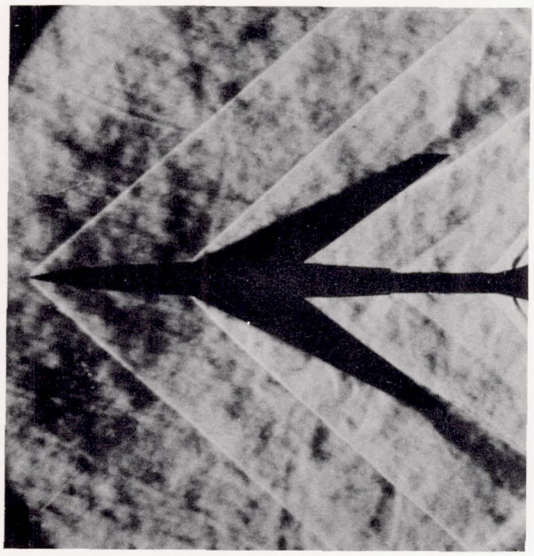

(f) WF–63; C_L, 0.21.

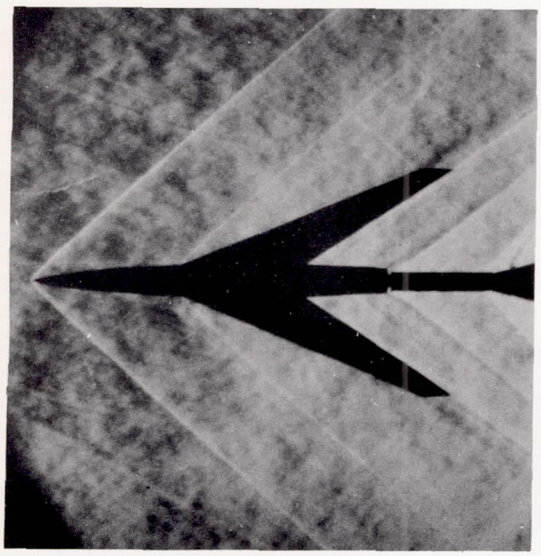

(g) WF–67; C_L, 0.

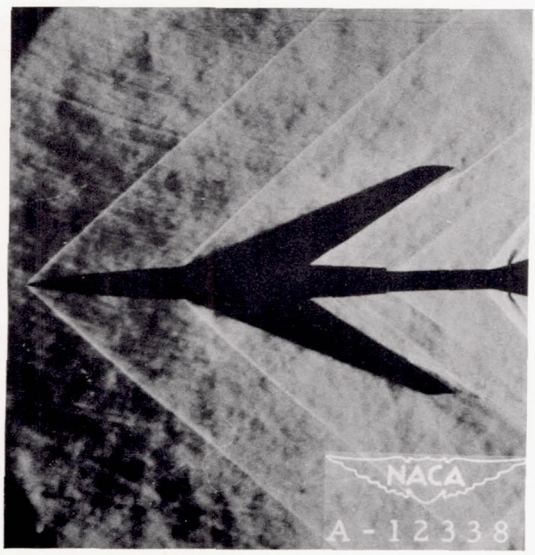

(h) WF–67; C_L, 0.22.

Figure 16.– Continued.

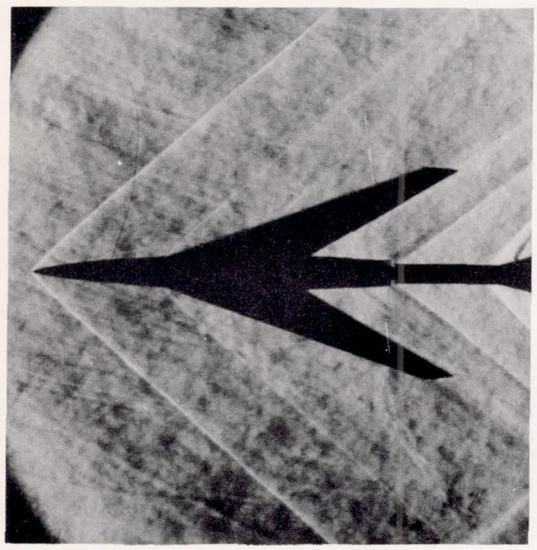

(i) WF-70; C_L, 0.

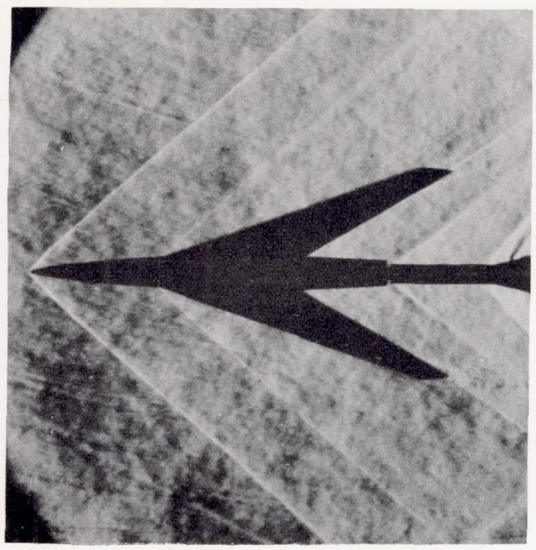

(j) WF-70: C_L, 0.21.

Figure 16.- Concluded.

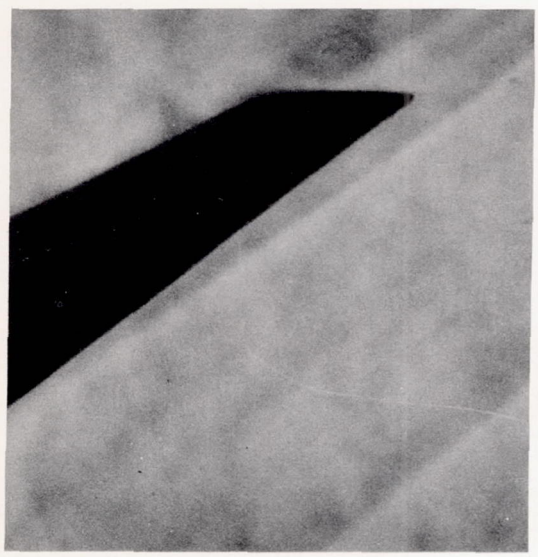

(a) R, 0.31 million.

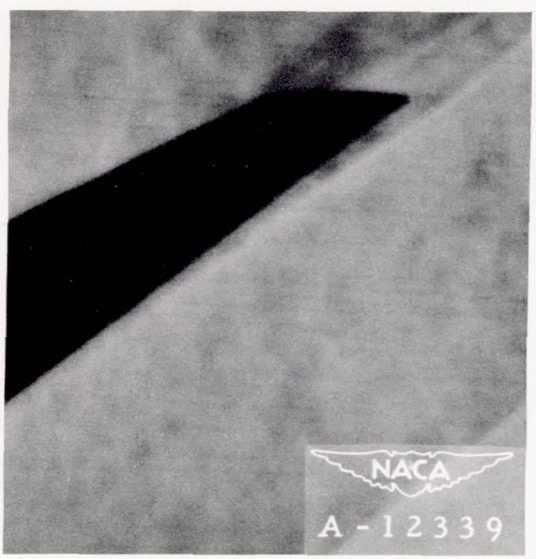

(b) R, 0.62 million.

Figure 17.- Schlieren photographs of WF-63 wing-tip flow patterns at zero lift.